# Design of Integrated Optoelectronic Switch

## M.Tech. Thesis

By

**Jogi Sri Nageswara Satya Aditya**

**DEPARTMENT OF ELECTRICAL ENGINEERING**

**INDIAN INSTITUTE OF TECHNOLOGY INDORE**

**June 2022**

# Design of Integrated Optoelectronic Switch

**A THESIS**

*Submitted in partial fulfillment of the*
*requirements for the award of the degree*
***of***
**Master of Technology**

*by*
**Jogi Sri Nageswara Satya Aditya**

**DEPARTMENT OF ELECTRICAL ENGINEERING**
**INDIAN INSTITUTE OF TECHNOLOGY INDORE**
**June 2022**

# INDIAN INSTITUTE OF TECHNOLOGY INDORE

## CANDIDATE'S DECLARATION

I hereby certify that the work which is being presented in the thesis entitled **Design of Integrated Optoelectronic Switch** in the partial fulfillment of the requirements for the award of the degree of **MASTER OF TECHNOLOGY** and submitted in the **DEPARTMENT OF ELECTRICAL ENGINEERING, Indian Institute of Technology Indore**, is an authentic record of my own work carried out during the time period from June 2021 to June 2022 under the supervision of Prof. Mukesh Kumar, Professor, Indian Institute of Technology Indore.

The matter presented in this thesis has not been submitted by me for the award of any other degree of this or any other institute.

J. Aditya
06/06/2022

**Signature of the student with date**
**(Jogi Sri Nageswara Satya Aditya)**

---

This is to certify that the above statement made by the candidate is correct to the best of my/our knowledge.

**06-06-2022**
Signature of the Supervisor of
M.Tech. thesis (with date)
**(Prof. Mukesh Kumar)**

---

**Jogi Sri Nageswara Satya Aditya** has successfully given his M.Tech. Oral Examination held on **06/06/2022**.

Signature(s) of Supervisor(s) of M.Tech. thesis
Date: **06-06-2022**

Convener, DPGC
Date: 06/06/2022

Signature of PSPC Member #1 06.06.2022
Date:

(A.K. Kashyap)
Signature of PSPC Member #2
Date: 07/06/2022

---

# ACKNOWLEDGEMENTS

I would like to sincerely thank **Prof. Mukesh Kumar**, my thesis supervisor and advisor for the last two years of my M.Tech. He has been very supportive since day one and I am grateful to him for devoting his time in guiding and motivating me to make the right decision when overwhelmed with options, or in moments of distress. I am thankful to him for providing me with the opportunities that shaped my M.Tech to be as it is today. I would also like to thank all **ONRL** members for their technical guidance and support during M.Tech thesis project.

I am grateful to my PSPC members **Prof. Vimal Bhatia** and **Dr. Ajay Kumar Kushwaha** for their cooperation and insightful comments on my research work and kindly going through my dissertation.

I sincerely acknowledge the support of **IIT Indore** and **MHRD** for supporting my M.Tech. by providing lab equipment and facilities, and TA scholarship, respectively.

Last but not the least, my work would not have been possible without the encouragement of my parents **Mr. Rambabu Jogi** and **Mrs. Kusuma Kumari Jogi**, whose tremendous support helped me stay positive and overcome the worst of hurdles. To them, I will forever be grateful. My heartfelt regards to my sisters **Ms. Praveena Jogi** and **Ms. Manasa Jogi**. I am thankful to both of you for believing in me and giving me emotional support, no matter which path I chose in life. Words are not enough to say how grateful I am to both of you.

**Aditya Jogi**

***Dedicated to***

***My Father Shri Rambabu Jogi***

# Abstract

Processing data at optical wavelengths has a number of advantages, particularly in terms of bandwidth and light is believed to be one of the most promising possibilities for replacing electronic signals as information carriers. Photonic devices are quickly gaining importance as potential saviors for meeting bandwidth demands in communication networks and high-speed computing. Silicon photonics offers a viable foundation for constructing highly scalable, low-cost on-chip photonic devices. However, Si photonics has a poor electro-refractive effect associated with a larger footprint, losses, and high energy consumption. As a solution, Si photonics is looking for a low-cost active material that can be used in conjunction with Si to achieve critical performance parameters. Graphene has unique electrical and optical properties, making it a good candidate for use as an active material in silicon photonics to improve light modulation, switching, and detection. Ring resonators serve a key role in lowering the size of Si photonics. In this thesis, a nanophotonic switch based on an electrically tunable graphene-silicon ring resonator is proposed and optical switching is realized by tuning the resonant wavelengths of the ring resonator. The shift in resonant wavelengths of the ring is achieved through modulation of the Fermi energy level of graphene by means of electrical gating. The hybrid plasmonic structure of the ring confines the light in nanoscale dimensions. The gap and length of the ring are optimized for a better extinction ratio. At a wavelength of 1550 nm, the proposed optical switch has an extinction ratio of 10.94 dB. A minimum gap of 100 nm and a smaller ring radius of 3.1 μm offers a minimal footprint area. The real and imaginary parts of the effective index of the ring w.r.t voltage across the graphene are observed. The results pave the path for more optical switches, and modulators based on electrically

controllable characteristics of the graphene and the ring resonator. The proposed design finds applications in optical interconnects, optical SRAM's and other integrated photonic devices.

# TABLE OF CONTENTS

# LIST OF FIGURES

# LIST OF TABLES

# NOMENCLATURE

| | |
|---|---|
| $\epsilon$ | Dielectric Constant |
| $\lambda$ | Wavelength |
| $\omega$ | Angular Frequency |
| $\mu$ | Permeability Constant |
| $\hbar$ | Reduced Planck's Constant |
| $\beta$ | Propagation Constant |
| $\Phi$ | Phase Shift |
| $E_F$ | Fermi Energy Level |
| $K_o$ | Free Space Wave Number |
| $\omega_p$ | Plasma Frequency |
| e | Charge of the Electron |
| $n_e$ | Electron Density |
| $m_e$ | Effective mass of Electron |
| $n_{eff}$ | Effective Refractive Index |
| L | Propagation Length |
| $\alpha$ | Transmission Coefficient |
| Q | Quality Factor |
| E | Electric Field Intensity |
| D | Density of States |

# ACRONYMS

| | |
|---|---|
| SPP | Surface Plasmon Polariton |
| MOS | Metal Oxide Semiconductor |
| MIM | Metal Insulator Metal |
| IMI | Insulator Metal Insulator |
| HPW | Hybrid Plasmonic Waveguide |
| PIC | Photonic Integrated Circuit |
| FOM | Figure Of Merit |
| WDM | Wavelength Division Multiplexing |
| $SiO_2$ | Silicon Dioxide |
| MRR | Micro Ring Resonator |
| ITO | Indium Tin Oxide |
| ENZ | Epsilon Near Zero |
| FDE | Finite Difference Eigenmode (FDE) solver |

# Chapter 1

# Introduction to Integrated Nanophotonics

## 1.1 Integrated Photonics

The insatiable demand for high-speed data, low power consumption and computational power pushes us to make better devices. Data intensive applications like artificial intelligence and machine learning process a large amount of data in real-time and current semiconductor electronic technology, cannot fulfill these demands. Scaling down electronic device dimensions has led to significant improvement in terms of speed, power consumption, cost and footprint area. However, devices can't be further scaled down due to several short channel effects and electronics are approaching their fundamental speed and bandwidth limitations, which is an increasingly serious problem that impedes further advances in many areas of modern science and technology. Today, commercial high-performance processors offer a compute power to memory bandwidth ratio of 5–10 TDP-FLOP/Byte [1] and this shows the need to increase the bandwidth. Due to electronic interconnect delay time issues and losses, achieving quicker electronic circuits running above 10 GHz is a major challenge. Photonic devices are savior devices for such problems and light is believed to be one of the most promising possibilities for replacing electronic signals as information carriers [2]. However, photonic devices are large and bulky and do not satisfy the demand for less footprint area and integration on a single chip is not possible. The advancement in the photonics lead to a new branch called Nanophotonics. This leads to the study of controlling and guiding light beyond its diffraction limitation. Figure 1.1 shows a Photonic Integrated Circuit (PIC) depicting the integration of photonic devices on a single chip with electronics. The elements of PICs are connected via waveguides which confine and direct light. The chip elements can be both passive (for e.g., couplers, filters, and multiplexers) and active (for e.g., modulators, switches, amplifiers, and detectors) [3]–[5]. These components are integrated and fabricated onto a single substrate, which creates a compact and robust photonic device. This integration dramatically improves the performance and reliability of photonic functions while simultaneously reducing the size, weight, and power consumption. Photonic devices find applications in energy-efficient lighting, high performance computing, environmental monitoring, chemical, and biological sensing and many more [6].

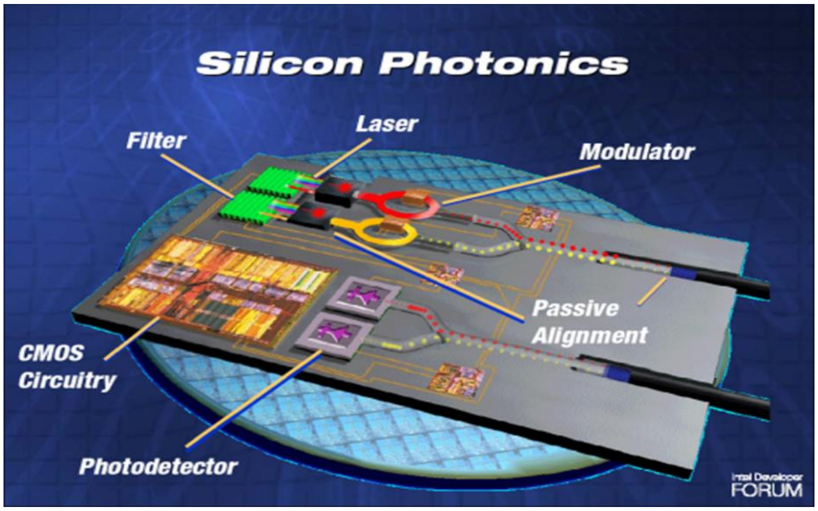


Figure 1.1 A Si photonic integrated circuit depicting the integration of photonic components with CMOS circuitry [7].

## 1.2 Nanophotonic devices and applications

The ability to control light matter interaction at the scale of a fraction of a wavelength of light has given rise to the area of photonics commonly known as Nanophotonics. The plasmons, slot waveguide, and photonic crystals are the few waveguides engineered device technologies that enable us to have devices much smaller than the dimensions of wavelength [8]. These devices have certain drawbacks like propagation losses and crosstalk due to leakage across the nano dimension device. Hybrid Plasmonic Waveguide (HPW) is proven to be a promising candidate in confining the light in deep subwavelength region and offering low propagation losses combining the properties of both Surface Plasmon Polariton (SPP) and photonic waveguides [9]. In nanophotonic devices, the light-matter interaction is large and larger the interaction, the easier it is to control and make better functional devices with high efficiency. The devices like optical switches, interconnects, modulators, polarization controllers, and memory are the few examples of such controlling and manipulating of the light using nanophotonic devices. Nanophotonic devices finds applications in almost all the fields but not limited to data centers, quantum computing, aeronautics, defense, biosensors and telecommunications [10], [11].

## 1.3 Types of Nanophotonic waveguides

The guiding and controlling of the light beyond the diffraction limit is crucial to make the photonic devices comparable to the size of modern on-chip electronic counterparts. In this section, some basic nanophotonic waveguide structures will be discussed.

### 1.3.1 Plasmonic waveguides

Surface plasmons are the free-electron gasses present on the surface of the metal. The coupling of electromagnetic wave with surface plasmons excite them which then start oscillating in sync with the electromagnetic wave to form a surface wave called as Surface Plasmon Polariton (SPP) [12]. The SPP exists only at the interface of metal and dielectric. SPP has a number of unique features, and can be of great importance for practical applications. Unlike dielectric waveguides where light confinement is limited by diffraction, plasmonic waveguides can "squeeze" light to a subwavelength scale [13]. This offers the possibility of scaling down photonic devices to the size of transistors which may result in successful integration of photonics and electronics. Though the field of plasmonics has several advantages it suffers from large ohmic losses. Metals have complex permittivity in optical region hence SPPs have a large propagation loss. This is a major limitation that has prevented plasmonics from becoming a more useful technology [14]. Surface plasmons have a direct relation between material property and incident light which makes it easy to control and manipulate. These properties made plasmonic waveguide a better candidate for the on-chip nanophotonic device in the application

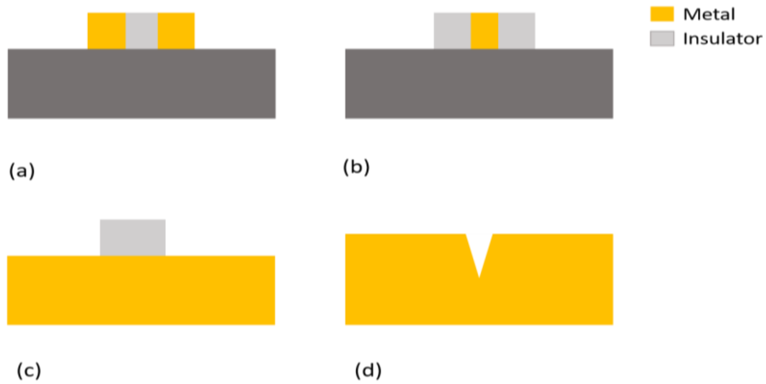


Figure 1.2 Various types of plasmonic waveguide (a) MIM (b) IMI (c) dielectric-loaded plasmonic waveguide (d) V grove MIM

of optical modulation, switching, sensing and photodetection [15]. To overcome ohmic losses, several plasmonic waveguide structures such as MIM metal-insulator-metal, MIS metal insulator semiconductor, V-grove MIM, IMI, etc., are proposed and few of them are as shown in Figure 1.2

#### 1.3.1.1 Surface Plasmon Polariton

The study of plasmonics deals with the generation, control, detection of plasmons as information carriers. Plasmons are the collection of charge carriers with quanta energy of $\hbar\omega_p$, where $\omega_p$ is the plasma frequency and it gives the effect of applying external electric field on the plasmon characteristics given by equation (1.1) [16]; $\hbar$ is the Planck's constant

$$\omega_p = \left(\frac{n_e\, e^2}{m_e\, \epsilon_0}\right)^{1/2} \tag{1.1}$$

Where e is the electrons electric charge, $m_e$ is the effective mass and $n_e$ is electrons density. The carrier density of metal is usually $10^{22}$

$cm^{-3}$ and for highly doped semiconductor is $10^{19}$ $cm^{-3}$. These high density of electrons acts as plasmons which oscillate at plasma frequency $\omega_p$, typically for metal its value is $10^{15}$ Hz. The interaction of plasmons and photons at the metal-dielectric boundary results in surface plasmon polariton (SPP) as shown in Figure 1.3. It depicts a metal-dielectric boundary where the medium for z > 0 is a lossless dielectric with permittivity $\epsilon_d$ and the medium for z < 0 is a metal with permittivity $\epsilon_m$. SP mode is always transverse magnetic TM in nature. The surface plasmon polariton SPP can bound the light in a few nanometers at the surface of the metal interface [17]. This can be utilized to scale down the photonic device size up to much extent. Thus, the SPP combines the benefit of the electronics and photonics to realize the nanophotonic devices.

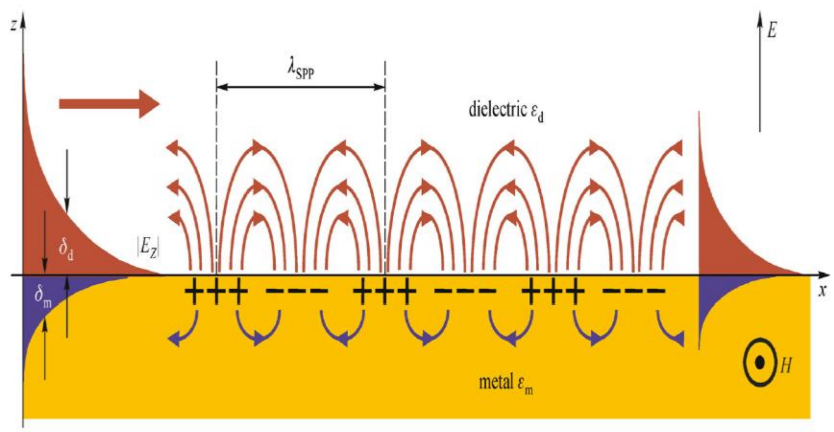


Figure 1.3 Schematic representation of field variation of surface plasmon polariton (SPP) at the metal-dielectric surface [1].

The expression for the dispersion relation of the SP mode [16] for the dielectric-metal boundary shown in Figure 1.3 is as given below

$$\beta = k_0 \sqrt{\left(\frac{\epsilon_1 \, \epsilon_2}{\epsilon_1 \, + \, \epsilon_2}\right)} \tag{1.2}$$

Where β is the propagation constant in the x direction and $k_0 = {}^{2\pi}/_{\lambda_0}$ is the free space wave number; wavelength in free space is denoted by $\lambda_0$. The permittivity of a lossless metal in the optical region [16] is given by the Drude model as

$$\epsilon_2 = 1 - \frac{{\omega_p}^2}{\omega^2} \tag{1.3}$$

Here ω is the angular frequency of light and $\omega_p$ is the plasma frequency of the metal. Substituting the expression of equation (1.3) for $\epsilon_2$ in equation (1.2), we obtain the dispersion relation of SP for a lossless dielectric-metal boundary.

$$\beta = k_0 \sqrt{\left(\frac{\epsilon_1 \left(1 - \frac{{\omega_p}^2}{\omega^2}\right)}{\epsilon_1 + 1 - \frac{{\omega_p}^2}{\omega^2}}\right)} \tag{1.4}$$

β is very close to $k_0\sqrt{\epsilon_1}$ for smaller values of ω. In this case the SP wave penetrates the dielectric to a great depth. As ω moves closer to the surface plasmon frequency ($\omega_{SP}$), β gets closer to infinity. This phenomenon is known as surface plasmon resonance [16]. The wave slows dramatically at the surface plasmon resonance frequency, and the field on either side of the interface becomes extremely small i.e., for short wavelengths the SP mode is confined closer to the surface and the distance of propagation is small and as the wavelength is increased, the SP is less confined and hence the propagation distance is increased.

#### 1.3.1.2 Losses in Plasmonic Waveguides

The plasmonic waveguide suffers from various metallic losses due to radiative and dephasing by inter electron collision and by generating hot electrons. These hot electrons radiate their energy in the form of heat thereby losing all energy which leads to high losses and small propagation length in the plasmonic waveguide. These energy dissipation of SPP leads to localized heating of the on-chip devices. To address this problem, a variety of ways have been suggested.

**a)** Use of gain medium: An optical gain medium can be used to reduce or eliminate the propagation loss of SP. Since SPs suffer significant propagation loss, the gain medium provides enough amplification to realize appreciable propagation [18]. Although gain assisted SPs have great potential, on-chip integration of gain medium with a plasmonic waveguide is not always simple, and this approach may not be the best solution for many applications [19].

**b)** Cryogenic cooling: The resistance of metal which is the source of SP propagation loss results from the random motion of electrons inside a metal. With a reduction of temperature, the random motion of electron and hence the propagation loss of SP is reduced [13]. Maintaining very low temperatures in a compact and cost-effective manner is challenging.

**c)** Improved plasmonic waveguide design: All plasmonic guides have a balance between loss and confinement. Increase in confinement is always accompanied by increase in propagation loss. However, the level of this compromise is not same for all types of plasmonic guides [20]. Many different types of plasmonic guides have been designed to obtain a good balance between confinement and loss.

### 1.3.2 Hybrid Plasmonic waveguides

To overcome various losses in the plasmonic waveguide a new hybrid device is proposed by the researchers where the plasmonic losses are compensated by coupling the modes i.e., optical mode and plasmonic mode resulting in a hybrid plasmonic mode [21]. The Hybrid plasmonic waveguide is a combination of two waveguides i.e., plasmonic waveguide and dielectric waveguide. It comprises of a silicon-based high-index region isolated from a metal surface by a low-index spacer (SiO2) as shown in Figure 1.4(a). Because of the close proximity of the metal-dielectric interface and the silicon slab, the SP mode and the dielectric waveguide mode supported by these two structures are coupled as shown in Figure 1.4(b). This configuration provides the advantages of both the waveguides i.e., low loss propagation of the signal and tight confinement in nano low index material. Because of these benefits, the hybrid plasmonic configuration has attracted the attention of researchers in the field of integrated nanophotonics [22]. Coupling the light from the source to the plasmonic waveguide is a major issue and the HPW has also solved

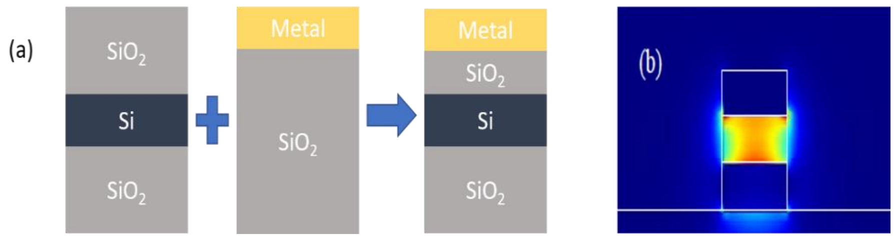


Figure 1.4 (a) Hybridization of Silicon photonic waveguide and plasmonic waveguide resulting in the hybrid plasmonic waveguide. (b) Mode confinement in the hybrid plasmonic waveguide showing maximum intensity in the dielectric layer [16].

this issue. The large light-matter interaction also helps in this waveguide for the application in optical modulation through the external electrical field. Various types of HPW are proposed in the literature and few of them are as shown in Figure 1.5.

The mode factor defines the quality of the hybrid mode as given by equation (1.5) [16]. It defines the figure of merit in terms of how much SPP energy and Optical energy couples together.

$$|a(d,h)|^2 = \frac{n_{hyb}(d,h) - n_{spp}}{\left(\left(n_{hyb}(d,h) - n_{cyl}(d)\right) + \left(n_{hyb}(d,h) - n_{spp}\right)\right)} \qquad (1.5)$$

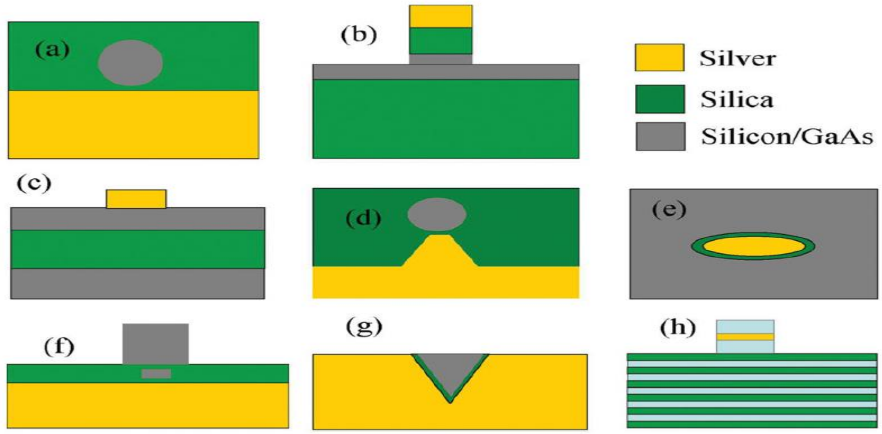


Figure 1.5 Various types of Hybrid Plasmonic Waveguides (HPW) [9].

|a| is the mode factor for the hybrid plasmonic waveguide $n_{hyb}$, $n_{spp}$ and $n_{cyl}$ are the effective refractive index of the hybrid mode, metal-dielectric plasmonic mode and optical mode respectively.

$$A = \frac{1}{max\{W(r)\}} \int W(r)\, dA \tag{1.6}$$

The effective mode area is given by equation (1.6). It defines the area of maximum energy density. W(r) is energy density per unit length along the propagation direction. The true figure of merit for hybrid plasmonic mode is defined by the ratio of how long the light can travel and how tightly the mode is constrained in the waveguide. FOM is given by

$$FOM = \frac{L}{\sqrt{A_{eff}}} \tag{1.7}$$

## 1.4 Ring Resonator and its Applications

### 1.4.1 Background and Motivation

Optical communication has progressively replaced electrical transmission over the last many decades. Tolerance to electromagnetic interference, minimum channel losses for large data speeds across long distances and high bandwidth capabilities per cable are all advantages of optical signaling over electrical transmission [23]. The benefits of photonics over electronics become obvious for smaller and smaller distances as communication bandwidth requirements continue to rise. Despite the multiple obstacles that short-reach electrical interconnects encounter, optics has typically remained absent from this sector because of the large number of optical components required per chip and their associated bulkiness. Passive silicon waveguide architectures, particularly wavelength selective devices and ring resonators, have demonstrated an extraordinary reduction in waveguide footprint [24], [25]. Photonic waveguides can have bend radii of less than 5 μm because of the large $n_{eff}$ contrast between silicon and its oxide (or air), allowing for incredibly compact rings. Ring resonators are crucial to the growth of silicon photonics because they enable on-chip integration of photonic devices.

### 1.4.2 Introduction to Ring Resonator

Integrated ring resonators have evolved in integrated photonics in recent years and have made their way into a variety of applications. MRR is a resonant cavity formed by a waveguide coiled around in a ring. The ring resonators use a parallel coupling waveguide to couple light from a straight waveguide to a circular shaped waveguide [26]. The distance between the interaction length and the ring is kept such that the desired frequency can be coupled into the ring. For optical feedback, integrated ring resonators don't need facets or gratings, making them ideal for monolithic integration with other components. A basic structure of the micro ring resonator is as depicted in Figure 1.6. MRRs find applications in optical sensors, filters, switches, optical amplifiers, routers and optical sources. The ring resonator is a key building block of a DWDM link. Unlike conventional WDM multiplexers, which use clunky arrayed waveguide gratings [27], that are hundreds of micrometers on a side, ring radii in DWDM links are on the order of 5 μm, allowing thousands of MRRs to be packed onto a single die.

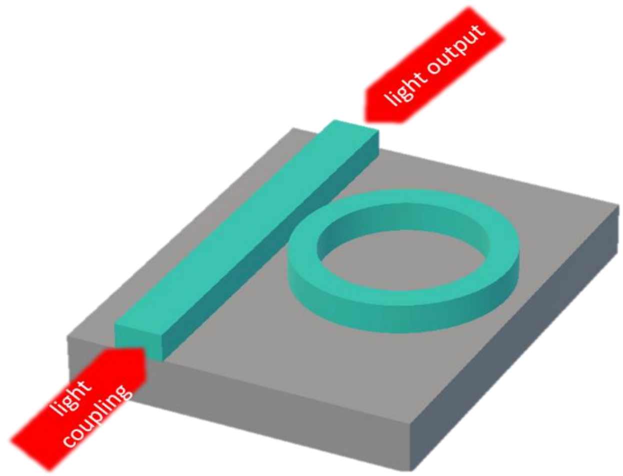


Figure 1.6 A basic structure of the microring resonator

### 1.4.3 Applications of Ring Resonator

Ring resonators have wide range of applications as shown in Figure 1.7. Ring resonators have been primarily investigated to be implemented as optical add–drop filters in optical networks. Several optical filter designs have been proposed and realized in semiconductors like purely passive devices, ring resonators with integrated gain sections and devices made out of active material. Optical filters need to be tunable in order to be deployed in optical networks and when it comes to ring resonators, the resonances of the ring resonator filter can be easily tuned. The researchers offer numerous manufactured devices that can be used for flexible dispersion compensation using ring resonators [28]. A square frequency response is essential in wavelength division multiplexing (WDM) applications. By combining a modified Mach–Zehnder interferometer (MZI) with a ring resonator, periodic multiplexers and demultiplexers with a flat passband and a large rejection region can be achieved. Ring resonators with very small radii have been developed thanks to advances in fabrication technique, allowing these elements to be used as modulators as well as logic gates and switching devices in optical signal processing systems [29].

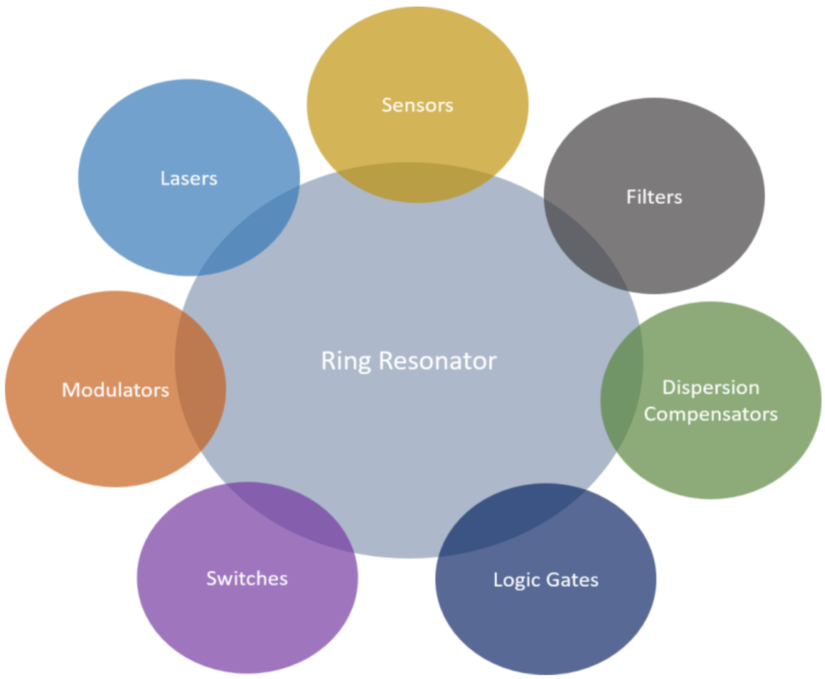


Figure 1.7 Ring resonator applications

Finally, as a latest technological movement known as Biophotonics emerges, MRRs have resurfaced in the form of sensors in this new field.

## 1.5 Graphene and its role in Si-based Nanophotonics

Si photonics have poor electro-refractive effect associated with larger footprint, losses and high energy consumption. As a result, Si photonics is on the lookout for a low-cost active material that can be coupled with silicon in achieving key performance metrics and advances in photonics are frequently driven by the material discovery and development that have special and unique properties [30]. Recently, one particular type of material, graphene has gained attention for on-chip active silicon photonics. Graphene a 2-D allotrope of carbon, consisting of carbon atoms packed in a hexagonal structure is as shown in Figure 1.8, has

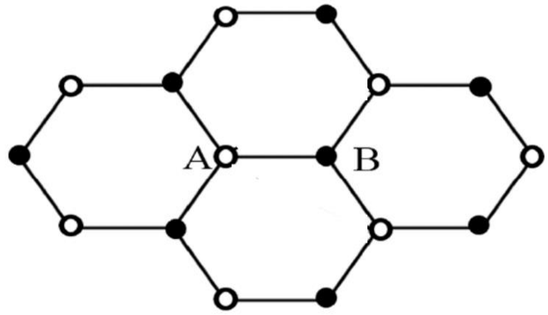


Figure 1.8 Graphene's honeycomb lattice structure. A and B denote carbon atoms in the unit cell [31].

exclusive electro-optical properties useful in a variety of photonic applications. Graphene is a zero-bandgap semiconductor whose fermi level can be adjusted by electrical gating [32] which results in a change in $n_{eff}$ and this property makes graphene to be used as an active material in silicon photonics to achieve more efficient light modulation, switching and detection. The complete band structure of graphene is as depicted in Figure 1.9. The Fermi-level coincides with the

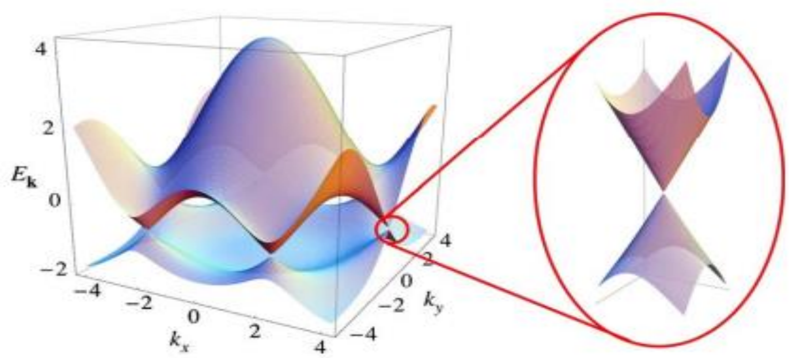


Figure 1.9 Complete band structure of graphene, inset shows the energy bands near the Dirac point [31].

Dirac point, where the totally filled valence band and the vacant conduction band coincide with zero band-gap. The Figure 1.9 inset shows that energy bands at the Dirac points are linear, as well as the fact that graphene is a semimetal, or a semiconductor with a zero-band gap [33]. Because of the 2D confinement of electrons and graphene's unique band structure, the interaction of graphene with electromagnetic radiation is noteworthy.

Since electrostatic gating alters the position of the Fermi energy, it provides a helpful knob for modulating optical absorption and this property makes graphene an interesting material and is used as an active material in various photonic devices like optical modulators, switches and photodetectors. From ultraviolet to terahertz, graphene interacts with electromagnetic radiation. Graphene is a strong contender for photonic applications because of its extensive interaction with light and unique electrical characteristics.

## 1.6 Organization of the Thesis

The thesis is organized in five chapters starting with an introduction to integrated nanophotonics and literature survey, one chapter consisting of the original research work followed by the conclusion and the future scope.

**Chapter 2 Literature Survey:** In this chapter, a brief literature review of the dielectric, plasmonic, hybrid plasmonic waveguides and ring resonators and graphene based nanophotonic applications is presented, which includes many currently reported works.

**Chapter 3 Optical Switching based on Ring Resonators and Graphene:** The third chapter covers the conceptual overview of nanophotonic devices including plasmonic waveguide, hybrid plasmonic waveguide, ring resonator and their applications. It also covers electrical and optical properties of graphene.

**Chapter 4 Electrically Tunable Nanophotonic Switch:** In this chapter, the proposed nanophotonic switch based on electrically tunable graphene-silicon ring resonator is presented. Graphene is incorporated in the ring resonator to achieve an extinction ratio of 10.94 dB at a wavelength of 1550 nm. The real and imaginary parts of the $n_{eff}$ of the ring w.r.t voltage across the graphene are analyzed.

**Chapter 5 Conclusion and Future Scope:** This chapter outlines the thesis and briefly discusses the future scope of the project.

# Chapter 2

# Literature Review

## 2.1 Introduction

Scaling down electronic device dimensions has led to improved speed, power consumption, cost and footprint area. However, devices can't be further scaled down due to several short channel effects hence the integration of modern electronic devices for information processing and sensing is rapidly approaching its fundamental speed and bandwidth limitations which is an increasingly serious problem that impedes further advances in many areas of modern science and technology [34]. Hence, new devices like double gate, gate all around transistors and FinFet are developed to satisfy the insatiable demand for speed and lower power consumption. With advanced MOS device and multi core compute architectures to achieve higher degree of parallelism, computing power significantly improved but clock frequencies are difficult to scale up. This shows the need to scale up bandwidth to meet the higher data rate requirements of data intensive applications like artificial intelligence, machine learning so that the overall clock frequency of the system improve. One of the most promising solutions is believed to be in replacing electronic signals as information carriers by light [11]. Photonic devices facilitate high operation speed due to high optical frequencies and possess a large data-carrying capacity owing to the huge photonic bandwidth.

Silicon photonics provides a promising platform for developing highly scalable, and potentially low-cost on-chip photonic devices. However, Si photonics has a poor electro-refractive effect associated with a larger footprint, losses, and high energy consumption. Hence, Si photonics is finding an effective low-cost active material that can be combined with Si in achieving key performance metrics. Graphene has unique electrical and optical properties which can be used as active material in silicon photonics to achieve more efficient light modulation, switching, and detection. Ring resonators play a significant role in reducing the footprint area of Si photonics [35]. In this chapter, recent works related to hybrid plasmonic waveguides along with electro-optical switches based on ring resonators and hybrid materials like graphene are reviewed.

## 2.2 Review on Optical Switches

Realizing a fully functional PIC requires on-chip optical functions like switching, detection and modulation. Ring resonators are important in Si photonics because they help to reduce the device footprint thus achieving the objectives towards on-chip photonics. Many research papers are devoted to ring resonator based optical switching and few of them will be discussed in this section.

**V. Van et.al-2002** [36] In GaAs ring resonators, they presented the first experimental instances of all photonic switching. The resonator's refractive index changes as a result of free carriers produced due to photon absorption, allowing switching to occur. This changes the wavelength of the probe out and into resonance. The deployed vertically connected MRR notch filter has a radius of 10 µm. Probe beam switching times of around 100 ps have been reported.

**Po Dong et.al-2010** [35] reported a thermally programmable silicon resonator with a tuning power of only 2.4 mW. Micro-heaters, that are put at the top of the device as a heat source with adequate isolation to prevent optical loss, are used to generate resonance shift. Thermal tuning exploits the large thermo-optic response of silicon hence changing the effective index and thereby the spectral response.

**Linjie Zhou et.al-2006** [37] reported a silicon electro-optic modulator based on microdisk resonator of ten micron diameter along with a laterally integrated p-i-n diode. serving as a heater, surrounding essentially the entire microdisk. The resonance modes are actively switched by means of introducing free carriers from an integrated p-i-n diode configuration that has the heavily-doped portions in the ring resonator core region. For a forward bias of 0.85 V across the p-i-n diode, a shift of 0.06 nm is seen.

**Nebiyu A. Yebo et.al-2010** [38] reported a microring resonator of 5 μm radius coated with colloidal droplets of ZnO nanoparticles with a diameter of roughly 3 nm. Through evanescent field interaction, the change in ZnO $n_{eff}$ caused by vapor adsorption alters the MRR resonance. This device can be utilized as a gas sensor to detect ethanol vapor levels as low as 100 ppm.

**M.A. Swillam et.al-2019** [39] reported ITO layer based hybrid plasmonic MRR that modulates the light signal by electrically stimulating carriers in the indium tin oxide (ITO), to approach the Epsilon-Near-Zero (ENZ) state, the resonance condition shifts, and the hybrid plasmonic MRR losses greatly increase. The extinction ratio is maximized while the insertion loss is minimized with this approach. The variation in Q with ring radius is reported and a insertion loss of 1.64 dB is reported with a 1 μm ring radius.

**X. Xiao et.al-2012** [40] presented a zigzag p-n junction based Si MRR modulator. High-speed modulation of 20 and 44 Gb/s with extinction ratios of 3.45 and 3.01 dB is experimentally demonstrated with a voltage swing of 3 V, indicating considerable promise in the application of ultrahigh-capacity optical interconnects.

**J.K. Rakshit et.al-2013** [41] reported an all-optical switch based on a MRR for logic and arithmetic operations. Switching is achieved through carrier injection in a GaAs–AlGaAs MRR. The MRRs resonant wavelength is shifted 1.5 nm using a green laser as an optical pump. Single ring as well as cascaded MRR simulation, analysis, and overall transfer function are investigated. A single circuit, comprised of three rings, is investigated and reported as being able to execute all of the 2 input 16 logic operations. The same circuit can also act as half adder/subtractor and single bit data comparator.

**A. Descos et.al-2016** [42] reported a Silicon photonics optical switch based on ring resonator with a radius of 14 μm. The resonant wavelength is blue-shifted as carriers are injected in the diode. This increases cavity losses and the Q factor is degraded. With a bias of 1V, a shift of 1.31nm is achieved.

## 2.3 Review on Graphene-based Nanophotonic Devices

Graphene has gained importance in nanophotonics due to its exclusive optical and electrical properties. Many Si nanophotonic devices using graphene as active material to overcome the weak electro-refractive effect of Si are proposed by researchers for efficient light modulation, switching, and detection. In this part, few of the graphene based nanophotonic devices in the literature will be reviewed.

**Majumdar et.al-2013** [43] demonstrated the integration of graphene with photonics is useful for electro-optic modulation. The cavity resonance is moved by 2 nm while electrostatically gating a single sheet of graphene on top of a photonic crystal cavity and the resonance reflectivity changes by about 400% (6 dB). This demonstrates a graphene–photonic crystal design with a small physical footprint could be helpful for low-power absorptive, refractive and high-speed applications.

**X. Gan et.al-2013** [44] reported electro-optic manipulation of a photonic crystal nanocavity coupled with an electrically gated monolayer graphene. At telecom wavelengths, tweaking the graphene layer's Fermi energy to 0.85 eV allows for robust regulation of its optical conductivity, permitting variation of cavity reflection in excess of 10 dB for a change in voltage of 1.5 V. The wavelength of the cavity resonance moves roughly 2 nm, and the quality factor increases thrice at 1570 nm.

**M. Liu et.al-2011** [45] reported a broadband electro-absorption modulator based on graphene. Monolayer graphene's $E_F$ is actively tuned to accomplish modulation. The electric field was maximized at the upper and lower surfaces of the silicon guide to further boost the electro-absorption modulation performance, and the inter-band transitions in graphene were also maximized. Under ambient conditions, the gigahertz graphene modulator reported a large electro-absorption modulation of 0.1 dB/μm and functions over a broad range of wavelengths from 1350 to 1600 nm.

**H. Dalir et.al-2016** [46] presented a graphene-based electro-absorption modulator with a modulation speed of 35 GHz, with absorption dynamically controlled by electrical gating of a double layer graphene to tune the $E_F$. Figure 2.1 exhibits the device design of high-speed broadband modulator. A 2 dB modulation depth was achieved within a band of photonic transmission wavelengths under ambient conditions (1500-1640 nm). More importantly, they have shown that

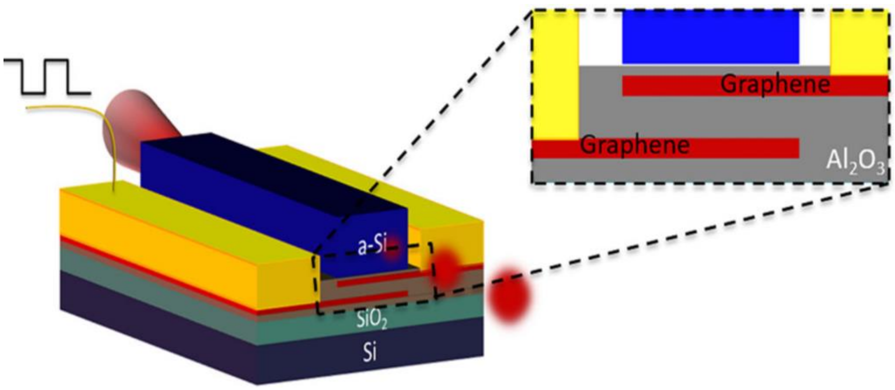


Figure 2.1 Cross-section schematic of the device depicting two graphene layers isolated by a 120 nm Al2O3 dielectric to form a capacitor [46].

the device's modulation output is unaffected by a broad range of temperature changes (25-145°C).

**Y. Hu et.al-2016** [47] presented a graphene-integrated silicon optical electro-absorption modulator with a modulation speed of 10 Gb/s. A 50 μm-long hybrid Si-graphene device was reported to have a minimum insertion loss of 3.8 dB at a wavelength of 1580 nm and a modest control voltage of 2.5 V, as well as thermal and broadband operation. The device's maximum modulation efficiency has been measured at 1.5 dB/V.

**V. SORIANELLO et.al-2016** [48] presented a Si ring resonator integrated with graphene as shown in Figure 2.1(a) and the complex optical conductivity of graphene on Si photonic waveguides was experimentally described which allows to precisely predict the behavior of PICs that include graphene sheets. By monitoring the shift in resonance and the

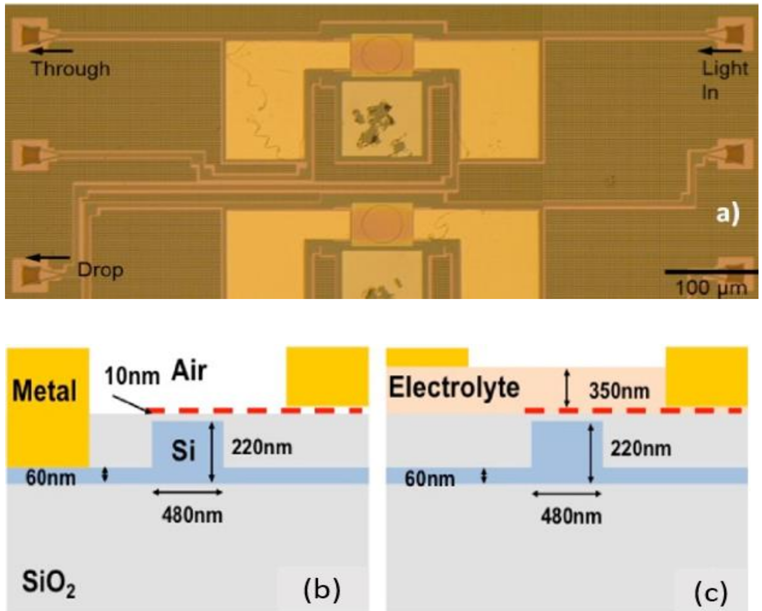


Figure 2.2 (a) SEM image of the graphene integrated MRR. Cross sections for two different gating strategies: Si gating (b), Electrolyte gating (c) [48].

variation in the drop maximum transmission, the influence of electrical gating of graphene on the complex $n_{eff}$ of the waveguide is described. For the first time on a Si photonics waveguide, the electro-refractive impact of graphene causes a massive (> $10^{-3}$) change in the $n_{eff}$. Two separate studies with two different gating strategies are considered: Si gating through the ridge waveguide and polymer-electrolyte gating as depicted in Figure 2.2(b) and 2.2(c). Both experiments show a considerable phase effect, which is consistent with numerical simulations.

**M.A. Giambra et.al-2020** [49] presented growth, transfer and fabrication protocols for integrating graphene into photonic devices providing ultrahigh (≥5000 $cm^2\ V^{-1}\ s^{-1}$) mobility and consistent efficacy at the wafer scale. This method uses chemical vapor deposition (CVD) to create single layer graphene matrices with up to twelve thousand unique single crystals that are created to sync with the geometrical structure of the PIC components. This is accompanied by a transfer strategy that ensures 80% coverage of the device area and wafer integrity up to 150 mm. This technique yielded double single layer graphene electro-absorption modulators with modulation efficiencies of 0.25, 0.45, 0.75 and 1 dB $V^{-1}$ for device lengths of 30, 60, 90, and 120 μm. Data speeds of approximately 20 Gbps are possible. This method is fully automated, allowing for mass production of graphene-based photonic devices.

## 2.4 Research Objectives

After doing the deep literature survey on the past works related to novel waveguiding schemes, optical switches, and MRRs I found the following area of improvement and worked through that.

Following are the objectives of the research work carried out for this thesis:

1. To utilize the exclusive electrical and optical properties of graphene to overcome the weak electro-optical effect of silicon.
2. To design an electrically tunable ring resonator based on hybrid plasmonic concept for achieving nanoscale confinement.
3. Design and analyze an electro-optic switch based on ring resonator and integrate graphene into the ring to explore the effect of gate tunability property of graphene on the ring resonance.

# Chapter 3

# Optical Switching based on Graphene and Ring Resonators

## 3.1 Optical Switches

An optical switch is a photonic device that is used to switch light on and off. With the increase of optical interconnects in datacenters, cloud environments and high-performance computers, the demand for a fully integrated optical switch technology is increasing. They enable reconfiguration of high-bandwidth data streams at a potentially lower cost and better power efficiency than conventional electrical switches. Additionally, using wavelength division multiplexing (WDM), multiple data streams can be routed together using a single optical device. Electro-optical switches provide a better control mechanism to easily control optical signal by means of electrical gate voltage as shown in Figure 3.1. Ring resonators have shown to be good candidates for high-speed switching and high integration due to a small form factor [50]. Several mechanisms like plasma dispersion effect, thermo-optic effect and more recently hybrid materials like graphene, ITO are used to change the effective refractive index of the resonator thereby shifting the resonance in

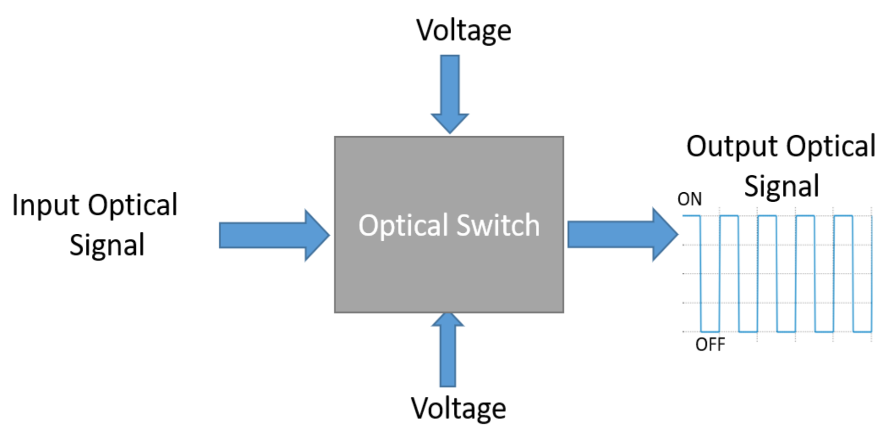


Figure 3.1 Electro-optical Switch illustrating optical switching by means of electrical voltage applied

and out of the input bus waveguide frequency thus switching the optical signal on and off. Figure 3.2 shows the basic switching mechanism in a ring resonator. Applying suitable ON bias voltage ($V_{bias\ ON}$) would turn

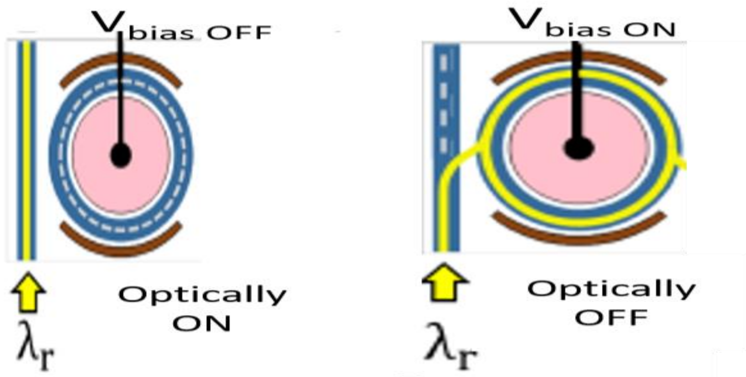


Figure 3.2 Schematic illustrating the basic switching mechanism using MRR as optical switch [51].

ON the resonator and the resonator resonance matches with input light wavelength and the light couples with the ring so the light does not reach the throughput port hence the switch is said to be in optically OFF state whereas suitable OFF bias voltage ($V_{bias\ OFF}$) would turn OFF the ring by shifting the resonance away from the input light hence optical signal is not coupled into the MRR and the input light reaches the throughput port hence the switch is said to be in optically ON state.

## 3.2Key-Performance Parameters of Optical Switches

There are several figures of merit that decide the performance of an optical switch and some of those are listed as extinction ratio, optical bandwidth, insertion loss, device footprint and power consumption.

**Extinction Ratio:** It is one of the foremost vital figures of merit for an optical switch. It is defined as the ratio of two intensities: $I_{max}$-the intensity transmitted when the switch is in ON state and $I_{min}$-the intensity transmitted when the switch is in OFF state. It is represented in decibels and expressed as: $10\log(I_{max} / I_{min})$. A large extinction ratio is desirable.

**Optical Bandwidth:** It refers to the useful operational wavelength range of the device. A wide optical bandwidth is preferred. Ring resonators provide optical switching over a large bandwidth as their resonance wavelengths are easily tunable.

**Insertion Loss:** It considers the optical power lost when the switch is added into the photonic circuit. It is a passive loss which comprises reflection, absorption, and mode coupling losses.

**Device Footprint:** It is the footprint area occupied by the switch. Device footprint area should be as minimum as possible. Ring resonators with small radii have less device footprint hence making it suitable for on-chip nanophotonic applications.

**Switching Power:** This parameter becomes particularly important when optical interconnects are considered. It is the amount of power consumed for switching the optical signal on and off.

## 3.3Modeling of Ring Resonator

The basic configuration of a ring resonator, which consists of unidirectional coupling between a ring resonator with radius r and a waveguide, is described in Figure 3.3. The optical signal is shined at the Input port (In) which then couples with the ring depending on the resonant wavelengths of the ring and the uncoupled light is received at the Throughput port (Thru).

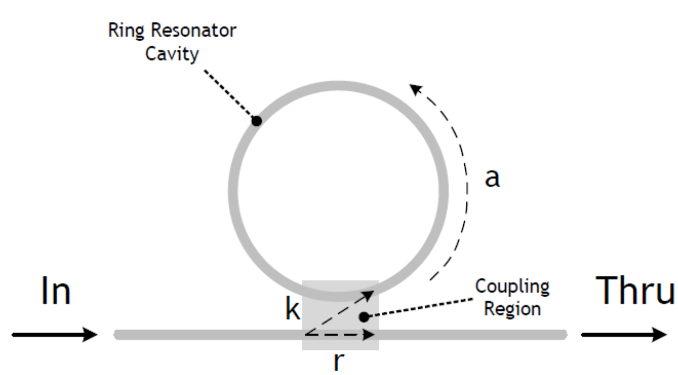


Figure 3.3 Microring resonator coupled to a bus waveguide through a coupling region.

The MRR's input port to through port transmission coefficient [52], α is specified by equation (3.1)

$$\alpha = \frac{I_{thru}}{I_{input}} = \frac{a^2 - 2ar\cos(\Phi) + r^2}{1 - 2ar\cos(\Phi) + a^2r^2} \tag{3.1}$$

where 'a' represents the MRR transmission for one roundtrip, 'r' denotes the bus waveguide's self-coupling, 'k' represents cross-coupling between the bus waveguide and the MRR. $r^2 + k^2 = 1$ as $r^2$, $k^2$ are the power splitting ratios of the coupler for a lossless coupling region.

The intensities at the input port and through port are $I_{input}$ and $I_{thru}$. The quantity Φ is equal to the microring waveguide's single-pass phase shift, which is specified by $\Phi = \beta L$. β is the propagation constant, which is equal to $2\pi n_{eff}L/\lambda$, and L is the microring's round-trip distance. Effective refractive index is $n_{eff}$.

When Φ is a multiple of $2\pi$, the ring is in resonance. For a set of resonant wavelengths, $\lambda_0$ this condition [52] is met.,

$$\lambda_0 = \frac{n_{eff}L}{m} \tag{3.2}$$

where m = 1,2,3………………

The transfer characteristics of the ring resonator are as shown in Figure 3.4. From in-port to through-port, MRR connected to a bus waveguide functions as a notch filter. Wavelengths that are not on resonance pass by the resonator, whereas wavelengths that are near to the $\lambda_o$'s are caught, and the resonances are periodic in nature.

The gap between resonances is called as the free spectral range (FSR) as shown in Figure. and is given by equation (3.3)

$$FSR = \frac{\lambda^2}{n_g L} \tag{3.3}$$

where $n_g$ is the group index, that accounts for the silicon waveguide's dispersion. When on resonance, equation (3.1) reduces to:

$$\alpha(\lambda_0) = 1 - A = \frac{a^2 - 2ar + r^2}{1 - 2ar + a^2r^2} = \frac{(a-r)^2}{1 - 2ar + a^2r^2} \tag{3.4}$$

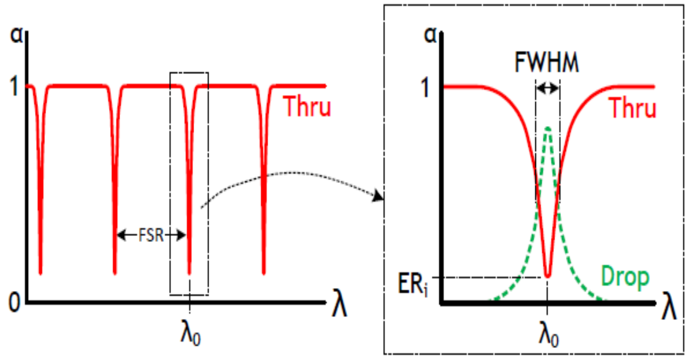


Figure 3.4 The optical transfer characteristics of a MRR that is resonant at $\lambda_0$ [52].

Once the ring is critically coupled, r = a and $\alpha(\lambda_0) = 0$ i.e., the power coupled from the bus guide equals the rate of decay of energy owing to losses in the ring. Substituting this condition in equation (3.4) we get

$$\alpha(\lambda_0) = \frac{(a-a)^2}{1-2a^2 + a^2a^2} = 0 \tag{3.5}$$

As a result, for a MRR to have the maximum extinction in its response, it must be critically coupled. However, because 'a' depends on the MRR loss, which is a result of various factors, 'r' and 'k' can be varied by adjusting the separation distance between the waveguide and MRR to tweak the percentage of evanescent wave coupling [52].

When the MRR is over coupled (r > a) or under coupled (r < a), $\alpha(\lambda_0) > 0$ Observe that in equation (3.4) when the ring is on resonance, a new quantity, 'A,' is defined, which relates to the reduction in through-port transmissivity (from unity). The intrinsic extinction ratio of a microring, $ER_i$, can also be defined as $ER_i = -10 \cdot \log_{10}(1-A)$ and $ER_i$ is infinite when the MRR is critically coupled.

The sharpness of the resonance and the MRRs selectivity are determined by the full-width half-maximum (FWHM) bandwidth, $\Delta\lambda$, of a microring around a resonance $\lambda_0$. This is given by equation (3.6)

$$\Delta\lambda = \frac{(1-ra){\lambda_0}^2}{\pi n_g L\sqrt{ra}} \tag{3.6}$$

Equation (3.7) relates the quality factor (Q-factor) of the ring and FWHM

$$Q = \frac{\lambda_0}{\Delta\lambda} \tag{3.7}$$

As losses in the microring increases, then ‘a’ which indicates round-trip transmission decreases, the ring has poorer resonance hence $\Delta\lambda$ increases as a result quality factor Q decreases. As a result, the ring's Q is inversely related to the ring cavity's loss. Doping the MRR in active configurations (modulators or a resonant photodetector, for example) reduces the Q by increasing round-trip loss owing to free carrier absorption. This process also establishes a bottom limit for the ring's radius; a radius that is too tiny will result in severe bend losses and a low-quality factor.

### 3.1.1 Resonance Tuning

From equation (3.2), the ring’s resonance is given by

$$\lambda_0 = \frac{n_{eff}L}{m}$$

The optical length L of a simple ring is the perimeter of the MRR, which is specified by $L = 2\pi R$, where R is the ring's radius. Therefore, $\lambda_0$ can be varied by adjusting the radius R and the $n_{eff}$ of the ring. Tuning resonance wavelengths by varying the radius is not a practically feasible solution after the ring is fabricated hence several mechanisms are proposed to modulate the resonance wavelengths of the ring by varying the effective refractive index. Many research papers proposed plasma dispersion effect based on depletion or injection of carriers to induce refractive index change. Variations in free carrier concentration are employed to tune $\lambda_0$ by varying the material’s $n_{eff}$ [53]. p-i-n junctions in carrier-injection modulators pump carriers into the intrinsic area during forward-bias, blue-shifting $\lambda_0$. p-n junctions in carrier-depletion modulators deplete the carriers from the junction during reverse bias, red-shifting $\lambda_0$. Electro-optic microring switch which modulates the resonance ($\lambda_0$) of the resonator to switch input light ON and OFF aligned close to $\lambda_0$ is as shown in Figure 3.5.

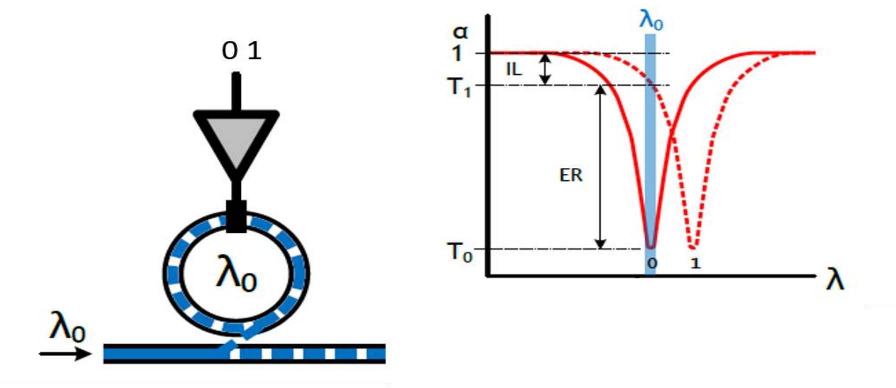


Figure 3.5 Transfer characteristics of ring resonator as an optical switch illustrating the tuning of ring resonance. The wavelength of the input light is the same as $\lambda_0$'s. T1 and T0 are the optical ones and zeros' output powers, normalized to the input power [52].

Here 0, 1 corresponds to two different sets of voltages applied to the ring, transfer characteristics of the ring is as shown in Figure 3.5 where the depleted state is represented by the 1 state, which is red-shifted in relation to the 0 state. Let's suppose the switch is turned off and the input light is the same wavelength as $\lambda_0$ at first so light is coupled into the ring and there is no output at the throughput port and on applying suitable voltage the resonance of the ring is shifted as indicated by state 1 in Figure 3.5 i.e., input light wavelength is not equal to $\lambda_0$ of the ring hence light is not coupled into the ring and is received at the throughput port. Thus, MRR can be used to switch light ON and OFF. Minority carrier lifetimes limit the speed of carrier-injection modulators; carrier-depletion designs avoid these concerns but necessitate mid-level doping control, which is challenging in a CMOS process. To eliminate these issues ring resonators based on active materials like graphene, ITO are proposed in the literature.

## 3.4 Graphene based Nanophotonic Devices

Photonics based on silicon (Si) is primarily used for downsizing and high-volume production of photonic integrated circuits. Si photonics encompasses both passive and active functions, such as waveguides and switching, detection, tuning, and modulation [54]–[58]. The plasma dispersion effect or the thermo-optical effect are the primary mechanisms for inducing absorption or, more significantly, index change in active Si photonics devices. Plasma dispersion is caused by fluctuations in free carrier density (accumulation, depletion, or injection) in Silicon doped regions, with the $n_{eff}$ change being largely influenced by hole density changes [59]. This phenomenon is exploited to modify the $n_{eff}$ of Silicon up to $\Delta n = 10^{-3}$ for a carrier concentration variation of the order of 5e17cm$^{-3}$, based on the carrier modulation mechanism. However, only in Silicon waveguides depending on the infusion or buildup of free carriers can such huge modifications be achieved. The index variation may be considerable in the event of injection, but the response is very sluggish (1ns) due to diffusion of carriers in the depletion area whereas in carrier accumulation, the $n_{eff}$ variation is considerable but the modulator is restricted by insertion loss caused by polySi section of the guide. The carrier depletion phenomenon in reverse biased pn junctions is used in silicon photonics phase modulators that require >20GHz bandwidth and low insertion loss. At 1550nm, the waveguide $n_{eff}$ variation is merely of order $\Delta n = 10^{-4}$ [54], hence these can be exceedingly rapid (ns). This lower value of $\Delta n$ is mostly linked to the extreme reverse bias which can be applied across pn junction without causing breakdown. The thermo-optical effect, on the other hand, can have a higher effect on index change due to Si's huge thermo-optic coefficient ($\Delta n/\Delta T = 1.8\text{x}10^{-4}$/K), however the thermo-optical effect is very sluggish (μs scale). In silicon photonics, graphene can be employed as an active material to produce more efficient light modulation, switching and detection. While graphene-based devices have a lot of potential for high-speed electronics, it's just recently been identified as a photonic material for future optoelectronic applications [45]. Furthermore, graphene is integrated into silicon photonic devices in a CMOS compatible manner. Graphene positioned on a silicon structure (e.g., photonic crystal) can generate variations in both absorption and $n_{eff}$, according to previous tests using a vertical illumination approach. Experiments and design-based examples of graphene on silicon waveguide modulators are published. The use of graphene in plasmonics is also proven, with extraordinarily high wave localization at the nanoscale and negligible losses. Graphene plasmonics has sparked a lot of interest, and it has a lot of potential uses in gate-tunable optoelectronic devices not limited to metamaterials, switches, filters, polarizers, nanoantennas and radiation apertures, phase shifters, modulators, photodetectors covering frequencies from THz to MIR [60].

### 3.4.1 Optical Properties of Graphene

Graphene is a 2D form of three-dimensional (3D) crystalline graphite made up of a single layer of carbon atoms organized in a hexagonal configuration. Graphene has gained a lot of attention since its discovery in 2004 due to its unusual electrical, thermal, mechanical, and optical properties [61]. The carrier mobility of graphene has been observed to be reaching 200,000 $cm^2/Vs$ which makes it suitable for high switching speed applications and at low temperatures fermi velocity ($\upsilon_F$) of $10^8$ cm/s. It has exceptionally high tensile strength. Graphene is a good conductor of heat and electricity and it is the thinnest 2D material ever known. Graphene's band structure is made up of a fully filled conduction band and a vacant valence band that cross linearly at the Dirac point. [62]. Electrostatic gating or, identically, electron/hole chemical doping can readily control the Femi-level, allowing for a great deal of control over its optical properties. Because of its linear band structure and intense coupling of Dirac Fermions with incident photons, graphene has exceptional optical features. Interband and intraband optical transitions contribute to graphene's capability to absorb light over a wide spectral range. Interband transitions are used to represent graphene absorption from visible to near infrared wavelengths, fine structural constants are used to explain it [33], [63]. The fine structure constant defines the absorbance of suspended single-layer graphene as $\pi\alpha$, where $\alpha = {e^2}/{\hbar c}$ is the fine-structure constant [33] and has a value of 1/137 and is a dimensionless number. "It's one of the greatest damn mysteries of physics: a magic number that comes to us with no explanation by man," Feynman said of the fine structure constant. When a light wave with an electric field component (E) and a frequency (ω) strikes a graphene layer perpendicularly, the incident energy is calculated as,

$$W_i = \frac{c}{4\pi} |E|^2 \tag{3.8}$$

The energy absorbed $W_a$ is given by Fermi's golden rule as

$$W_a = \frac{2\pi}{\hbar} |M|^2 D(E_k)\hbar\omega \tag{3.9}$$

where D represents the density of states at half of the incident radiation energy, $E_k = E/2 = \hbar\omega/2$. For two dimensional Dirac fermions in graphene, $D(\hbar\omega/2) = \hbar\omega/\pi\hbar^2 v_F^2$, the matrix element M [31] for the coupling of Dirac fermions in graphene with the electric field component is given by

$$|M|^2 = \frac{1}{8} e^2 {v_f}^2 \frac{|E|^2}{\omega^2} \tag{3.10}$$

Substituting equation (3.10) in equation (3.9) we get

$$W_a = \frac{2\pi}{\hbar} \frac{1}{8} e^2 {v_f}^2 \frac{|E|^2}{\omega^2} \frac{(\hbar\omega)^2}{\pi\hbar^2 {v_f}^2} \tag{3.11}$$

The amount of energy absorbed is expressed as a percentage and is given by

$$\frac{W_a}{W_i} = \pi\left(\frac{e^2}{\hbar c}\right) = \pi\alpha = 2.3\% \tag{3.12}$$

As a result, optical absorption is unaffected by incident frequency or material properties. The absorption rises with graphene thickness, with each layer adding 2.3 % to the total quantity of energy absorbed.

### 3.4.2 Gate Dependent Optical Transitions in Graphene

The optical response in far infrared region is due to the intraband transitions or free carrier absorption. External electric-field modulated conductivity is the basis of modern electronics. For low-dimensional materials, an external electric field shifts position of the Fermi level, resulting in change in the electric current. A gate voltage, like the knob on an electrical current, can be used to control the optical transmission of low-dimensional systems [61]. Graphene, dissimilar from other materials, exhibits significant variation of the optical transition due to electric field gating. The Fermi energy EF is shifted by the applied gate voltage, where $E_F = \pm n\hbar v_F$; 'n' is the carrier concentration dependent on the applied gate voltage [32]. Interband absorption is highly affected by electrostatic doping, and interband transitions with photon energy $<2E_F$ are blocked for hole-doped graphene while those with photon energy $> 2E_F$ are unaffected, as depicted in Figure 3.6. The IR absorption is dramatically modulated as a result of this, with a raise in absorption related to the shift in $E_F$. Because of the change in electronic band structure, gate driven IR absorption in bilayer graphene differs greatly from that in monolayer graphene. Optical transitions between two valence bands are permitted in hole-doped bilayer graphene. As hole doping increases, the emission becomes more noticeable due to a downshift in EF, allowing for larger leaps, as shown in Figure 3.6.

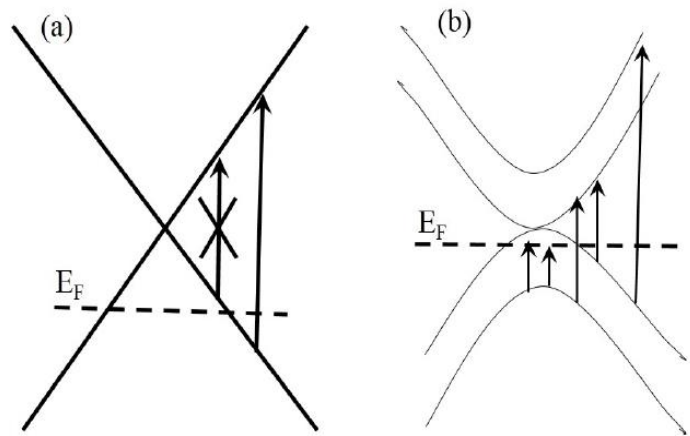


Figure 3.6 In (a) monolayer and (b) bilayer graphene, gate controllable interband transitions [31].

# Chapter 4

# Electrically Tunable Nanophotonic Switch

## 4.1 Introduction

Scaling down electronic device dimensions has led to significant improvement in terms of speed, power consumption, cost and footprint area. However, devices can't be further scaled down due to several short channel effects. Today, commercial high-performance processors offer a compute power to memory bandwidth ratio of 5–10 TDP-FLOP/Byte [1]. This shows the need to increase the bandwidth to meet the higher data rate requirements of data intensive applications like artificial intelligence, machine learning so that the overall clock frequency of the system improve. Due to electronic interconnect delay time issues and losses, achieving quicker electronic circuits running above 10 GHz is a major challenge. Light is believed to be one of the most promising possibilities for replacing electronic signals as information carriers. Optical devices facilitate high operation speed due to high optical frequencies and possess a tremendous data-carrying capacity because of the wide bandwidth [2], [34]. Photonic devices find applications in energy-efficient lighting, high performance computing, environmental monitoring, chemical, and biological sensing and many more. However, miniaturization of optical devices is a big challenge due to diffraction limitations in the subwavelength region. Hybrid Plasmonic Waveguide (HPW) is proven to be a promising candidate in confining the light in deep subwavelength region and offering low propagation losses combining the properties of both Surface Plasmon Polariton (SPP) and photonic waveguides [9], [23], [64]–[67].

Silicon photonics involving active functionalities like switching, tuning, modulation and detection the basic mechanism to induce refractive index change is plasma dispersion effect based on depletion or injection type p-n junctions. However, Si photonics have poor electro-refractive effect associated with larger footprint, losses and high energy consumption [68]. Graphene a 2D allotrope of carbon, made of carbon atoms packed in a hexagonal configuration, has unique electro-optical properties [61], [69] useful in a broad range of photonic applications. Graphene is a zero-bandgap semiconductor whose fermi level is adjusted through electrical gating which results in a change in refractive index. Graphene is used as an active material in Si photonics to achieve more efficient light modulation, switching and detection [70]–[74]. Furthermore, graphene can be integrated into silicon photonic devices in a CMOS compatible manner [60], [75].

Ring resonators serve a key role in lowering the size of Si photonics. An optical waveguide coiled back on itself forms a ring resonator, with a resonance happening when the resonator's optical length is an integer multiple of wavelengths [26], [50]. Ring resonators are extensively used in optical modulators/switches, optical filters, light sources and optical sensing [76]–[79]. Hybrid plasmonic MRRs are recently suggested as a viable alternative for achieving nanoscale light confinement [80]–[83].

In this work, a photonic switch based on electrically tunable graphene – silicon ring resonator is proposed. The suggested ring resonator shows electrically controllable characteristics taking advantage of gate tunability property of graphene. The Hybrid Plasmonic Waveguide (HPW) design of the ring tightly confines the mode in the nanoscale SiO2 layer by overcoming diffraction limitations. The subwavelength confinement and placing of graphene over the ring provide strong interaction of light with the graphene layer. In this work, we measured the shift in resonance wavelength of micro ring as a function of graphene gating. As, voltage is varied from 0 to -15 v, a maximum resonance wavelength shift of 2 nm is obtained. The variation in chemical potential of graphene w.r.t applied voltage is also observed. The coupling gap and length of the ring resonator are optimized for improving the Extinction Ratio (ER).

## 4.2 Proposed Device Design

The proposed electrically tunable optical switch is as shown in Figure 4.1. It is based on SOI architecture and consists of an input Si photonic waveguide which is connected to an output hybrid plasmonic waveguide via a tapered waveguide that converts photonic mode into a hybrid plasmonic mode. Input silicon bus waveguide's width and thickness are 450 nm and 220 nm, respectively. The hybrid plasmonic waveguide consists of a Metal-Insulator-Semiconductor (MIS) structure. Gold is preferred as it offers lower losses in near-infrared region [84], [85] and gold's thickness and width are selected to be 100 nm and 300 nm respectively. SiO2 being CMOS compatible is considered as the oxide layer and easily formed by Si oxidation, it's thickness and width are 20 nm and 300 nm. respectively. On a SiO2 substrate, a Si layer with width and thickness of 300 nm and 200 nm is constructed. A micro ring resonator having a similar MIS structure as the hybrid plasmonic waveguide with a radius of 3.1 um is designed. At the boundary of gold and SiO2, a single sheet of graphene is incorporated into the ring. The coupling length and gap between the hybrid plasmonic guide and ring are optimized for higher ER to be 1.5 μm and 100 nm. In the proposed hybrid plasmonic ring, light is tightly confined in the SiO2 dielectric layer thereby providing a significant coupling between the graphene and the light.

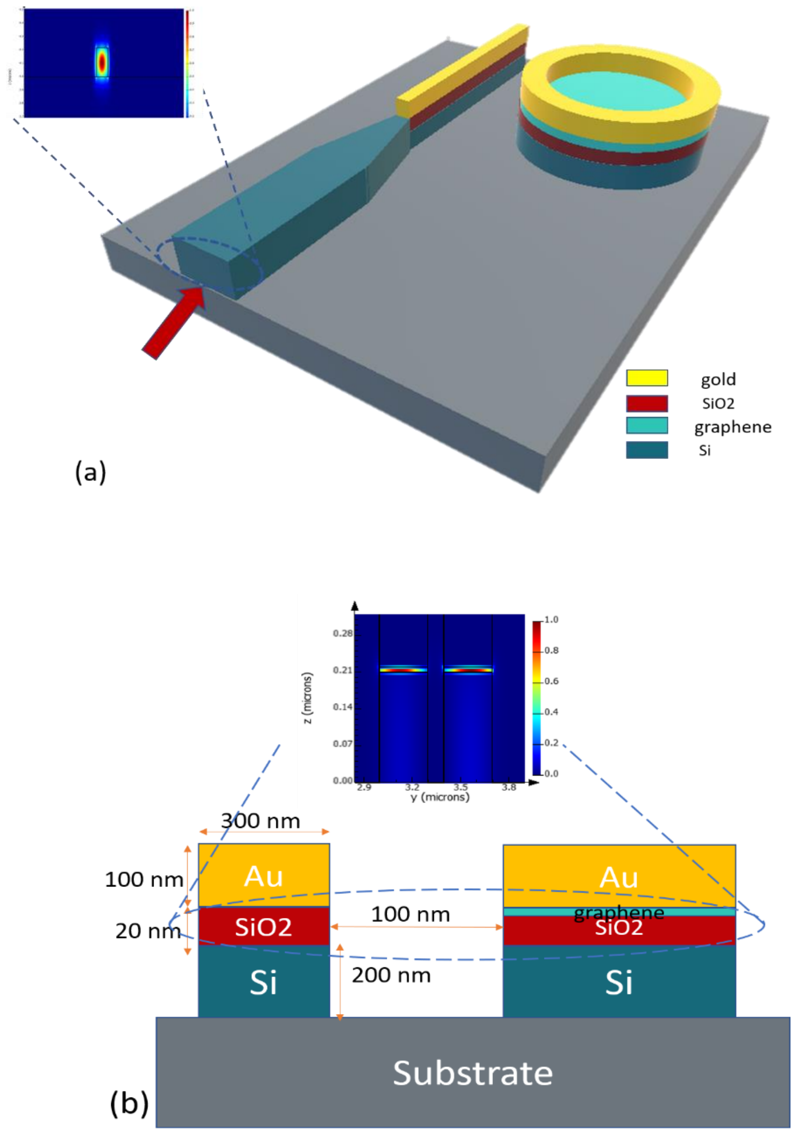


Figure 4.1 (a) Three-dimensional image of the proposed optical switch based on electrically tunable graphene- Si ring resonator; thickness of gold, SiO2, and silicon are 100, 20 and 200 nm respectively, inset shows the electric field confinement in 220 nm thick Si photonic waveguide, and (b) Cross section of the device shows the coupling region between ring and hybrid plasmonic waveguide separated by a gap of 100 nm, inset shows the electric field confinement in 20 nm thick SiO2 layer of hybrid plasmonic ring and the hybrid plasmonic waveguide.

## 4.3 Electrically Tunable Characteristics

The device design, simulation and analysis are done with Lumerical using Finite Difference Eigenmode (FDE) and Finite Difference Time Domain (FDTD) solvers. Figure 4.1 (a) inset depicts the photonic waveguide's electric field confinement. Figure 4.1 (b) inset shows field confinement in the HPW and the ring at the overlap region. This shows the strong confinement of the field with the graphene layer hence electrical gating of graphene effects the optical mode characteristics. Figure 4.2 (a) depicts the propagation of electric field down the waveguide when the ring is resonating i.e., ON resonance state (-15 v) and Figure 4.2 (b) depicts the field propagation when the ring is in OFF resonance state (-3 v). In the resonant state light gets coupled into the ring and resonates whereas in the OFF resonant state light is not coupled into the ring and reaches the throughput port.

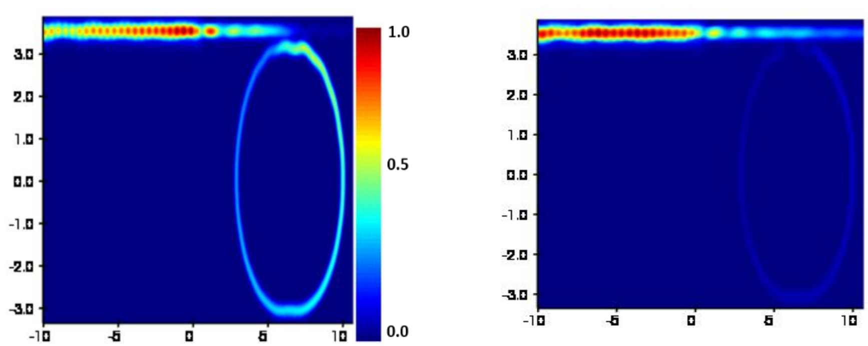


Figure 4.2 Electric Field propagation along the waveguide in (a) ON resonance state i.e., -15 v is applied across graphene, and (b) OFF resonance state i.e., -3 v is applied across graphene.

Electrical and optical properties of graphene are highly adjustable through electrostatic gating or doping which shifts the Fermi energy level (EF). Light resonating in the ring strongly interacts with graphene hence electron-hole pairs are generated. For a given input wavelength, carriers generated varies depending on position of the $E_F$ which results in a change in ηeff of ring thereby shifting resonant wavelengths of the ring w.r.t applied voltage across the graphene. This phenomenon of tuning the resonant wavelengths of the ring with applied voltage [86], [87] can be used to switch an optical signal on and off and hence this device can be utilized as a photonic switch Figure 4.3 shows the variation in chemical potential of graphene w.r.t applied voltage across graphene.

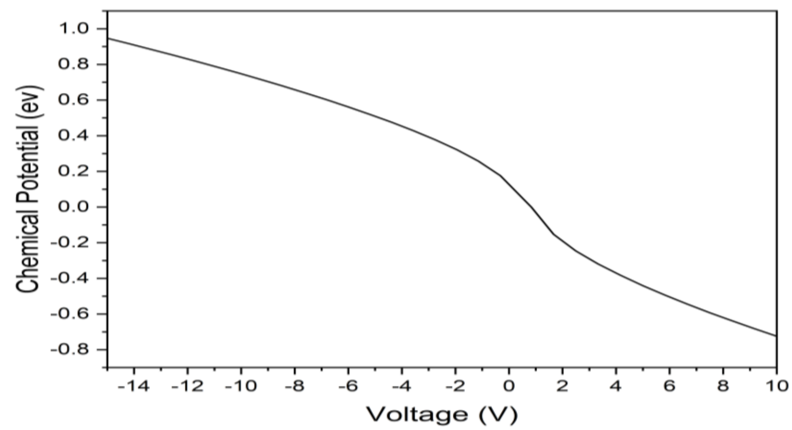


Figure 4.3 Variation in chemical potential of graphene with voltage applied across graphene; a change in chemical potential of 0.95 ev is observed for a 15-v change in voltage.

A change in chemical potential of 0.95 ev is observed for a 15-v change in voltage. The coupling length and the gap are highly optimized to achieve higher ER. The shift in resonance and ER for a

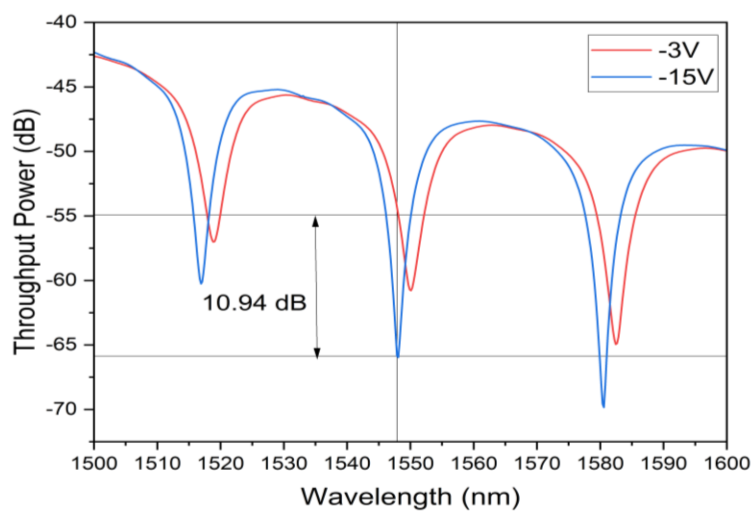


Figure 4.4 Throughput port power characteristics of the MRR showing the variation in resonance wavelengths of the ring with voltage applied across graphene; a shift in resonance of 2 nm and ER of 10.94 dB is observed for a 12-v change in voltage at 1550 nm.

fixed gap of 100 nm and various coupling lengths are shown in Table 1. A minimum gap of 100 nm is fixed to achieve less device footprint area and only the coupling length is optimized. The throughput port power versus the wavelength characteristics of the ring resonator for a coupling gap and length of 100 nm and 1.5 μm is as shown in Fig 4.4.

TABLE 4.1. Shift in resonance and ER for various coupling lengths

| S.N. | Length (μm) | ER (dB) | Shift in resonance (nm) |
|---|---|---|---|
| 1 | 0.9 | 5.87 | 1.2 |
| 2 | 1 | 6.39 | 1.84 |
| 3 | 1.5 | 10.94 | 2 |
| 4 | 2 | 10.01 | 1.9 |
| 5 | 2.5 | 9.372 | 1.3 |

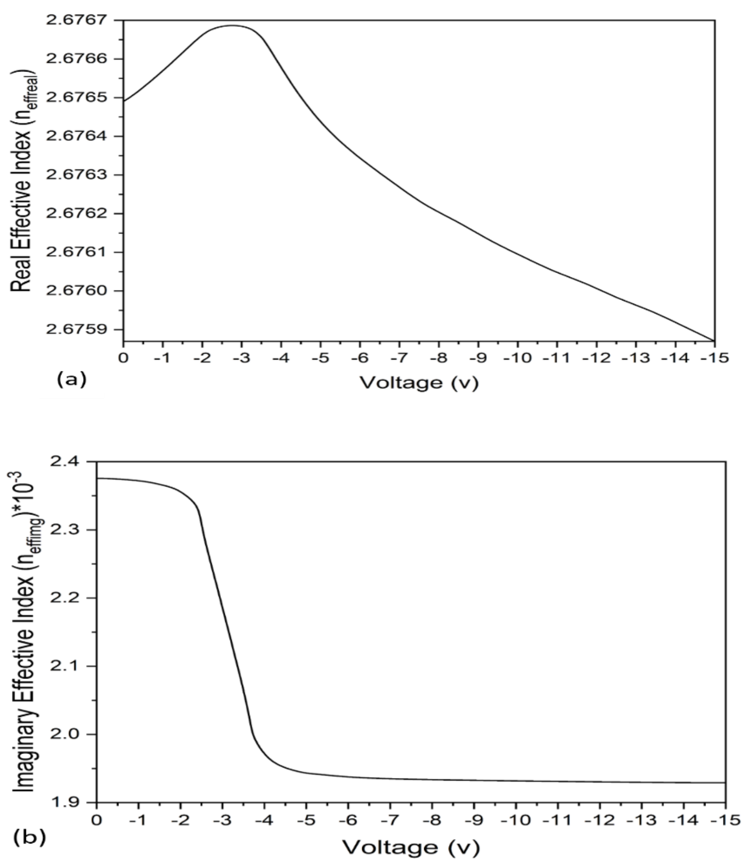


Figure 4.5 (a) Variation in real $n_{eff}$ with voltage applied across graphene, and (b) Variation in imaginary $n_{eff}$ with voltage applied across graphene, for a length and gap of 1.5 μm and 100 nm.

A resonance shift of 2 nm and an ER of 10.94 dB is observed. The real and imaginary $n_{eff}$ of the ring resonator for a length and gap of 1.5 μm and 100 nm are as depcited in Figure 4.5 (a) and Figure 4.5 (b). The real effective index indicates phase shift and is a measure of shift in resonance of the ring. From 0 to -3 v range which corresponds to a chemical potential of less than 0.4 ev we observe an increase in real effective index hence there is a red shift in resonance wavelengths whereas from -3 to -15 v range we observe a decrease in real effective index hence there is a blue shift in $\lambda_0$ as shown in Figure 4.6. The imaginary effective index indicates losses in the ring and for voltages less than -3 v there is a

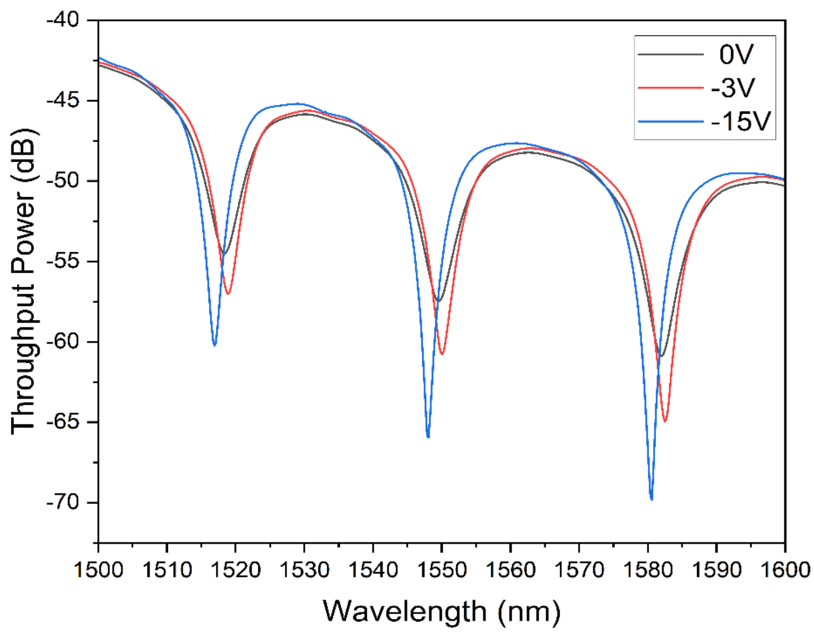


Figure 4.6 Throughput port characteristics of the ring resonator showing a red shift in resonance for 0 to -3 v range and red shift in resonance for -3 to -15 v.

decrease in imaginary effective index hence the losses decrease which is clearly evident from a sharper dip in the throughput port characteristics of Figure 4.4 i.e., the dip corresponding to -15 v is much sharper compared to -3 v indicating low losses and good resonance. The effect of integrating 2 single layers of graphene into the ring resonator is also investigated with one graphene layer at the gold-$SiO_2$ interface and other at the $SiO_2$ -Si interface. The two-layer graphene optical switch design is also optimized to achieve better extinction ratio by varying the coupling length between the bus guide and the MRR by keeping the gap to be 100 nm. The throughput characteristics of the ring are as shown in Figure 4.7.

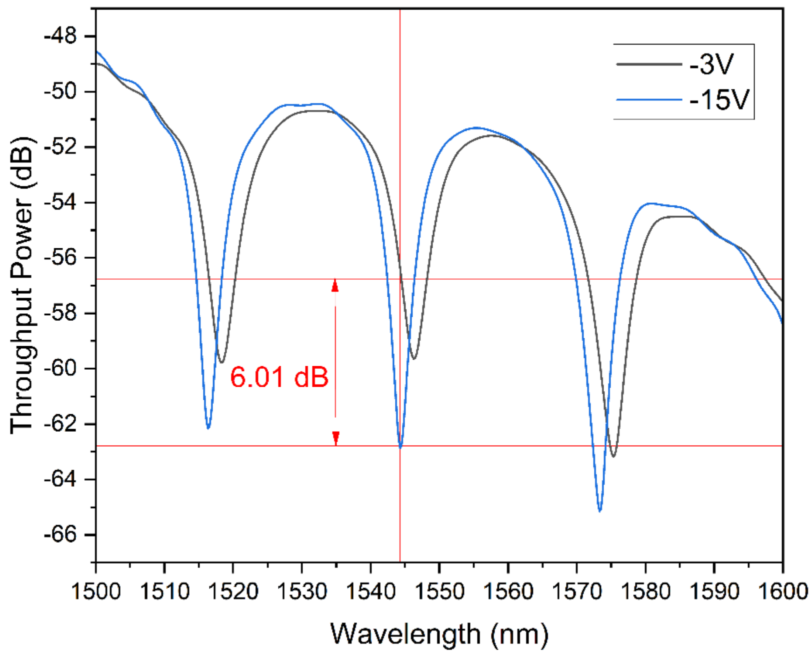


Figure 4.7 Throughput port power characteristics of the MRR showing the variation in $\lambda_0$ of the 2-layer graphene integrated ring with voltage applied across graphene; a shift in resonance of 1.8 nm and ER of 6.01 dB is observed for a 12-v change in voltage at 1550 nm.

The shift in resonance and ER for a fixed gap of 100 nm and various coupling lengths for a 2-layer graphene integrated ring are shown in Table 4.2. The maximum ER is observed to be 6.01 dB corresponding to a length of 1 μm and the shift in resonance is found to increase as length increases but ER increases. The ER is maximum for a single layer graphene MRR.

TABLE 4.2 Shift in resonance and ER of 2-layer graphene integrated ring for various coupling lengths

| **S.N.** | **Length (μm)** | **ER (dB)** | **Shift in resonance (nm)** |
|---|---|---|---|
| 1 | 0.9 | 5.64 | 1.2 |
| 2 | 1 | 6.01 | 1.8 |
| 3 | 1.5 | 4.3 | 2.02 |
| 4 | 2 | 3.39 | 2.17 |

## 4.4 Summary

A nanophotonic switch based on electrically tunable graphene-silicon ring resonator is proposed. Optical switching is realized by tuning the resonant wavelength of the guided hybrid plasmonic mode in MRR. The shift in resonant wavelengths of the ring is achieved through modulation of $E_F$ of graphene by means of electrical gating. The gap and length of the ring are optimized for improved extinction ratio of 10.94 dB at a wavelength of 1550 nm. A minimum gap of 100 nm and a smaller ring radius of 3.1 μm offers minimal footprint area. The $\eta_{effreal}$ and $\eta_{effimg}$ of the ring w.r.t voltage across the graphene is observed. The findings pave the way for more optical switches, modulators based on electrically controllable characteristics of the graphene and the ring resonator. The proposed design can be used in various applications like optical interconnects, optical SRAM's and other integrated photonic devices.

# Chapter 5

## Conclusion and Future Scope

Currently, Si nanophotonics is focused on two main objectives one is to reduce the size of nanophotonic devices that allows increased packaging density, which is vital on a chip and other is to overcome the weak electro-optic effect of Si. In the present thesis, Silicon photonics objectives have been incorporated in two ways, one is material engineering (i.e., introducing some other optoelectronic materials with Si to overcome major limitation of Si) and another one is device engineering (incorporating new device structure i.e., proposed device acts as an inherent optical mode converter thereby eliminating the need for grating couplers). A nanophotonic switch based on graphene-silicon ring resonator is designed and analyzed. In the aspect of material engineering, graphene has proven to be a viable material for very efficient optical modulation because of its electrically controllable Fermi energy level near-infrared wavelength and outstanding CMOS compatibility.

The major contribution of the thesis is summarized as follows:

- To achieve optical switching, an electrically tunable graphene-silicon based ring resonator is proposed. The variation in chemical potential of graphene with respect to different gate voltages is observed. The throughput port characteristics of the ring resonator for various applied gate voltages are discussed.
- The gate tunability property of graphene is explored to alter $n_{eff}$ in the ring resonator thereby tuning the resonance of the ring. Graphene is incorporated into the hybrid plasmonic ring resonator to guide the light at nanoscale and then control it electrically. Graphene-Silicon based hybrid ring resonator addresses the above listed major challenges of Si photonics i.e., graphene is introduced to overcome weak electro-optic effect in Si and a microring is used to minimize the size of photonic devices.

- Optical switching is realized by tuning the $\lambda_0$ of the guided hybrid plasmonic mode in ring resonator. The shift in resonant wavelengths of the ring is achieved through modulation of $E_F$ of graphene by means of electrical gating. The hybrid plasmonic structure of the ring confines the light in nanoscale dimensions. The gap and length of the ring are optimized for better extinction ratio. The proposed optical switch exhibits an extinction ratio of 10.94 dB at a wavelength of 1550 nm. A minimum gap of 100 nm and a smaller ring radius of 3.1 μm offers minimal footprint area. The real and imaginary parts of the $n_{eff}$ of the ring w.r.t voltage across the graphene is observed. The proposed design finds applications in optical interconnects, optical SRAM's and other integrated photonic devices.

Although, the proposed nanophotonic switch is designed to achieve better extinction ratio. Indeed, there remain several future possibilities to further accomplish and extend the objective of the thesis. Following are the future scope for the presented work:

- The thickness of Si and $SiO_2$ layers in the proposed device can be optimized in sync with coupling gap and length of the ring to study the effect on mode confinement which might result in better switching characteristics.
- The effect of doping graphene can also be considered as one of the possibilities to achieve higher extinction ratio.
- The length and width of the tapered waveguide can be adjusted to reduce the coupling losses due to mode conversion from photonic to hybrid plasmonic waveguide thereby improving the output power characteristics of the ring.
- Replacing $SiO_2$ with high-K dielectrics reduces any leakage currents thereby minimizing optical switching power.
- The proposed nanophotonic switch uses fabrication friendly photonic device components hence it can be used to design a optical

static random access memory (O-SRAM) with a smaller device footprint.

# REFERENCES

[1] J. Wang, “A review of recent progress in plasmon-assisted nanophotonic devices,” *Front. Optoelectron.*, vol. 7, no. 3, pp. 320–337, Sep. 2014, doi: 10.1007/S12200-014-0469-4.

[2] V. Kaushik *et al.*, “On-chip nanophotonic broadband wavelength detector with 2D-Electron gas Nanophotonic platform for wavelength detection in visible spectral region,” *Nanophotonics*, vol. 11, no. 2, pp. 289–296, Jan. 2022, doi: 10.1515/NANOPH-2021-0365/ASSET/GRAPHIC/J_NANOPH-2021-0365_FIG_004.JPG.

[3] H. W. Hübers, “Terahertz technology: Towards THz integrated photonics,” *Nat. Photonics*, vol. 4, no. 8, pp. 503–504, Aug. 2010, doi: 10.1038/NPHOTON.2010.169.

[4] M. U. Khan, Y. Xing, Y. Ye, and W. Bogaerts, “Photonic integrated circuit design in a foundry+fabless ecosystem,” *IEEE J. Sel. Top. Quantum Electron.*, vol. 25, no. 5, Sep. 2019, doi: 10.1109/JSTQE.2019.2918949.

[5] K. Ohashi *et al.*, “On-chip optical interconnect,” *Proc. IEEE*, vol. 97, no. 7, pp. 1186–1196, 2009, doi: 10.1109/JPROC.2009.2020331.

[6] A. Karabchevsky, A. Katiyi, A. S. Ang, and A. Hazan, “On-chip nanophotonics and future challenges,” *Nanophotonics*, vol. 9, no. 12, pp. 3733–3753, Sep. 2020, doi: 10.1515/NANOPH-2020-0204/ASSET/GRAPHIC/J_NANOPH-2020-0204_FIG_006.JPG.

[7] R. Katti and S. Prince, “A survey on role of photonic technologies in 5G communication systems,” *Photonic Netw. Commun.*, vol. 38, no. 2, pp. 185–205, Oct. 2019, doi: 10.1007/S11107-019-00856-W/FIGURES/18.

[8] S. Lal, S. Link, and N. J. Halas, “Nano-optics from sensing to waveguiding,” *Nat. Photonics 2007 111*, vol. 1, no. 11, pp. 641–648, Nov. 2007, doi: 10.1038/nphoton.2007.223.

[9] M. Z. Alam, J. S. Aitchison, and M. Mojahedi, “A marriage of convenience: Hybridization of surface plasmon and dielectric waveguide modes,” *Laser and Photonics Reviews*, vol. 8, no. 3. Wiley-VCH Verlag, pp. 394–408, 2014. doi: 10.1002/lpor.201300168.

[10] J. K. Doylend and A. P. Knights, “The evolution of silicon photonics as an enabling technology for optical interconnection,” *LASER PHOTONICS Rev. Laser Photonics Rev*, vol. 6, no. 4, pp. 504–525, 2012, doi: 10.1002/lpor.201100023.

[11] Z. Fang and C. Z. Zhao, “Recent Progress in Silicon Photonics: A Review,” *ISRN Opt.*, vol. 2012, pp. 1–27, Mar. 2012, doi:

10.5402/2012/428690.

[12] Y. Fang and M. Sun, “Nanoplasmonic waveguides: towards applications in integrated nanophotonic circuits,” *Light Sci. Appl. 2015 46*, vol. 4, no. 6, pp. e294–e294, Jun. 2015, doi: 10.1038/lsa.2015.67.

[13] R. F. Oulton *et al.*, “Plasmon lasers at deep subwavelength scale,” *Nat. 2009 4617264*, vol. 461, no. 7264, pp. 629–632, Aug. 2009, doi: 10.1038/nature08364.

[14] “Super Mode Propagation in Low Index Medium.” https://opg.optica.org/viewmedia.cfm?uri=CLEO-2007-JThD112&seq=0 (accessed May 31, 2022).

[15] C. Sirtori, S. Barbieri, and R. Colombelli, “Wave engineering with THz quantum cascade lasers,” *Nat. Photonics*, vol. 7, no. 9, pp. 691–701, Sep. 2013, doi: 10.1038/NPHOTON.2013.208.

[16] M. Z. Alam, “Hybrid Plasmonic Waveguides : Theory and Applications by © Copyright by Muhammad Zulfiker Alam , 2012 Hybrid Plasmonic Waveguides : Theory and Applications,” *Thesis*, 2012.

[17] D. Rioux, S. Vallières, S. Besner, P. Muñoz, E. Mazur, and M. Meunier, “An Analytic Model for the Dielectric Function of Au, Ag, and their Alloys,” *Adv. Opt. Mater.*, vol. 2, no. 2, pp. 176–182, Feb. 2014, doi: 10.1002/ADOM.201300457.

[18] K. Tetz, M. P. Nezhad, and Y. Fainman, “Gain assisted propagation of surface plasmon polaritons on planar metallic waveguides,” *Opt. Express, Vol. 12, Issue 17, pp. 4072-4079*, vol. 12, no. 17, pp. 4072–4079, Aug. 2004, doi: 10.1364/OPEX.12.004072.

[19] I. De Leon and P. Berini, “Amplification of long-range surface plasmons by a dipolar gain medium,” *Nat. Photonics 2010 46*, vol. 4, no. 6, pp. 382–387, Mar. 2010, doi: 10.1038/nphoton.2010.37.

[20] A. Boltasseva, T. Nikolajsen, K. Leosson, K. Kjaer, M. S. Larsen, and S. I. Bozhevolnyi, “Integrated optical components utilizing long-range surface plasmon polaritons,” *J. Light. Technol.*, vol. 23, no. 1, pp. 413–422, Jan. 2005, doi: 10.1109/JLT.2004.835749.

[21] R. F. Oulton, V. J. Sorger, G. Bartal, and X. Zhang, “A hybrid plasmonic waveguide for sub-wavelength confinement and long range propagation,” *Front. Opt. 2008/Laser Sci. XXIV/Plasmonics Metamaterials/Optical Fabr. Test. (2008), Pap. MTuD3*, p. MTuD3, Oct. 2008, doi: 10.1364/META_PLAS.2008.MTUD3.

[22] O. Benson, “Assembly of hybrid photonic architectures from nanophotonic constituents,” *Nat. 2011 4807376*, vol. 480, no. 7376, pp.

193–199, Dec. 2011, doi: 10.1038/nature10610.

[23] R. D. Mishra, L. Singh, S. Rajput, V. Kaushik, S. Srivastava, and M. Kumar, "Engineered nanophotonic waveguide with ultra-low dispersion," *Appl. Opt.*, vol. 60, no. 16, p. 4732, Jun. 2021, doi: 10.1364/ao.428534.

[24] W. Bogaerts *et al.*, "Compact Wavelength-Selective Functions in Silicon-on-Insulator Photonic Wires," *IEEE J. Sel. Top. QUANTUM Electron.*, vol. 12, no. 6, doi: 10.1109/JSTQE.2006.884088.

[25] E. Ryckeboer *et al.*, "Silicon-on-insulator spectrometers with integrated GaInAsSb photodiodes for wide-band spectroscopy from 1510 to 2300 nm," *Opt. Express, Vol. 21, Issue 5, pp. 6101-6108*, vol. 21, no. 5, pp. 6101–6108, Mar. 2013, doi: 10.1364/OE.21.006101.

[26] "Integrated Ring Resonators," *Integr. Ring Reson.*, 2007, doi: 10.1007/978-3-540-68788-7.

[27] P. Dumon *et al.*, "Compact wavelength router based on a Silicon-on-insulator arrayed waveguide grating pigtailed to a fiber array," *Opt. Express, Vol. 14, Issue 2, pp. 664-669*, vol. 14, no. 2, pp. 664–669, Jan. 2006, doi: 10.1364/OPEX.14.000664.

[28] K. K. Mehta *et al.*, "Polycrystalline silicon ring resonator photodiodes in a bulk complementary metal-oxide-semiconductor process," *Opt. Lett.*, vol. 39, no. 4, p. 1061, Feb. 2014, doi: 10.1364/OL.39.001061.

[29] M. Georgas, J. Orcutt, R. J. Ram, and V. Stojanović, "A monolithically-integrated optical receiver in standard 45-nm SOI," *Eur. Solid-State Circuits Conf.*, pp. 407–410, 2011, doi: 10.1109/ESSCIRC.2011.6044993.

[30] A. H. Castro Neto, F. Guinea, N. M. R. Peres, K. S. Novoselov, and A. K. Geim, "The electronic properties of graphene," *Rev. Mod. Phys.*, vol. 81, no. 1, pp. 109–162, Jan. 2009, doi: 10.1103/REVMODPHYS.81.109.

[31] M. K. Kavitha and M. Jaiswal, "Graphene: A review of optical properties and photonic applications," *Asian J. Phys.*, vol. 25, no. 7, pp. 809–831, 2016.

[32] F. Wang *et al.*, "Gate-Variable Optical Transitions in Graphene." [Online]. Available: https://www.science.org

[33] R. R. Nair *et al.*, "Fine structure constant defines visual transparency of graphene," *Science*, vol. 320, no. 5881, p. 1308, Jun. 2008, doi: 10.1126/SCIENCE.1156965.

[34] M. Paniccia, "Integrating silicon photonics," *Nature Photonics*, vol. 4, no. 8. pp. 498–499, Aug. 2010. doi: 10.1038/nphoton.2010.189.

[35] A. V. Krishnamoorthy *et al.*, “Wavelength-tunable silicon microring modulator,” *Opt. Express, Vol. 18, Issue 11, pp. 10941-10946*, vol. 18, no. 11, pp. 10941–10946, May 2010, doi: 10.1364/OE.18.010941.

[36] V. Van Member, T. A. Ibrahim, P. P. Absil, F. G. Johnson, R. Grover, and P. T. Ho, “Optical signal processing using nonlinear semiconductor microring resonators,” *IEEE J. Sel. Top. Quantum Electron.*, vol. 8, no. 3, pp. 705–713, May 2002, doi: 10.1109/JSTQE.2002.1016376.

[37] L. Zhou *et al.*, “Silicon electro-optic modulators using p-i-n diodes embedded 10-micron-diameter microdisk resonators,” *Opt. Express, Vol. 14, Issue 15, pp. 6851-6857*, vol. 14, no. 15, pp. 6851–6857, Jul. 2006, doi: 10.1364/OE.14.006851.

[38] N. A. Yebo, P. Lommens, R. Baets, and Z. Hens, “An integrated optic ethanol vapor sensor based on a silicon-on-insulator microring resonator coated with a porous ZnO film,” *Opt. Express, Vol. 18, Issue 11, pp. 11859-11866*, vol. 18, no. 11, pp. 11859–11866, May 2010, doi: 10.1364/OE.18.011859.

[39] M. M. Badr, M. M. Elgarf, and M. A. Swillam, “Silicon ring resonator electro-optical modulator utilizing epsilon-near-zero characteristics of indium tin oxide,” *Phys. Scr.*, vol. 94, no. 12, p. 125507, Sep. 2019, doi: 10.1088/1402-4896/AB3CF9.

[40] X. Xiao *et al.*, “44-Gb/s silicon microring modulators based on zigzag PN junctions,” *IEEE Photonics Technol. Lett.*, vol. 24, no. 19, pp. 1712–1714, 2012, doi: 10.1109/LPT.2012.2213244.

[41] J. K. Rakshit, T. Chattopadhyay, and J. N. Roy, “Design of ring resonator based all optical switch for logicand arithmetic operations - A theoretical study,” *Optik (Stuttg).*, vol. 124, no. 23, pp. 6048–6057, 2013, doi: 10.1016/J.IJLEO.2013.04.075.

[42] A. Descos *et al.*, “Silicon photonics optical switch based on ring resonator; Silicon photonics optical switch based on ring resonator,” 2016.

[43] A. Majumdar, J. Kim, J. Vuckovic, and F. Wang, “Electrical control of silicon photonic crystal cavity by graphene,” *Nano Lett.*, vol. 13, no. 2, pp. 515–518, Feb. 2013, doi: 10.1021/NL3039212/SUPPL_FILE/NL3039212_SI_001.PDF.

[44] X. Gan *et al.*, “High-contrast electrooptic modulation of a photonic crystal nanocavity by electrical gating of graphene,” *Nano Lett.*, vol. 13, no. 2, pp. 691–696, Feb. 2013, doi: 10.1021/NL304357U/SUPPL_FILE/NL304357U_SI_001.PDF.

[45] M. Liu *et al.*, “A graphene-based broadband optical modulator,” *Nat.*

*2011 4747349*, vol. 474, no. 7349, pp. 64–67, May 2011, doi: 10.1038/nature10067.

[46] H. Dalir, Y. Xia, Y. Wang, and X. Zhang, “Athermal Broadband Graphene Optical Modulator with 35 GHz Speed,” *ACS Photonics*, vol. 3, no. 9, pp. 1564–1568, Sep. 2016, doi: 10.1021/ACSPHOTONICS.6B00398/ASSET/IMAGES/LARGE/PH-2016-003987_0004.JPEG.

[47] Y. Hu *et al.*, “Broadband 10 Gb/s operation of graphene electro-absorption modulator on silicon,” *Laser Photon. Rev.*, vol. 10, no. 2, pp. 307–316, Mar. 2016, doi: 10.1002/LPOR.201500250.

[48] C. Huyghebaert *et al.*, “Complex effective index in graphene-silicon waveguides,” *Opt. Express, Vol. 24, Issue 26, pp. 29984-29993*, vol. 24, no. 26, pp. 29984–29993, Dec. 2016, doi: 10.1364/OE.24.029984.

[49] C. Coletti *et al.*, “Wafer-scale integration of graphene-based photonic devices,” *ACS Nano*, vol. 15, no. 2, pp. 3171–3187, Feb. 2021, doi: 10.1021/ACSNANO.0C09758/ASSET/IMAGES/LARGE/NN0C09758_0009.JPEG.

[50] W. Bogaerts *et al.*, “LASER & PHOTONICS REVIEWS Silicon microring resonators,” *Laser Photonics Rev*, vol. 6, no. 1, pp. 47–73, 2012, doi: 10.1002/lpor.201100017.

[51] R. Kudalippalliyalil, S. Chandran, A. P. Jacob, and A. Jaiswal, “Towards Scalable, Energy-Efficient and Ultra-Fast Optical SRAM,” pp. 2–6, 2021, [Online]. Available: http://arxiv.org/abs/2111.13682

[52] C. Sun, “Silicon-Photonics for VLSI Systems,” *Ph.D. Diss. Massachusetts Inst. Technol.*, no. 2009, 2015.

[53] R. A. Soref and B. R. Bennett, “Electrooptical effects in silicon,” *IEEE J. Quantum Electron.*, vol. 23, no. 1, pp. 123–129, 1987, doi: 10.1109/JQE.1987.1073206.

[54] G. T. Reed and A. P. Knights, “Silicon photonics : an introduction,” p. 255, 2004.

[55] R. Soref, “The Past, Present, and Future of Silicon Photonics,” *IEEE J. Sel. Top. QUANTUM Electron.*, vol. 12, no. 6, 2006, doi: 10.1109/JSTQE.2006.883151.

[56] “Silicon Photonics.” https://opg.optica.org/jlt/abstract.cfm?uri=jlt-24-12-4600 (accessed May 28, 2022).

[57] Y. Arakawa, T. Nakamura, Y. Urino, and T. Fujita, “Silicon photonics for next generation system integration platform,” *IEEE Commun. Mag.*, vol. 51, no. 3, pp. 72–77, 2013, doi: 10.1109/MCOM.2013.6476868.

[58] L. Pavesi and D. J. Lockwood, Eds., “Silicon Photonics III,” vol. 122, 2016, doi: 10.1007/978-3-642-10503-6.

[59] R. Soref and J. Larenzo, “All-silicon active and passive guided-wave components for λ = 1.3 and 1.6 µm,” 1986. doi: 10.1109/JQE.1986.1073057.

[60] H. Tian *et al.*, “Wafer-Scale Integration of Graphene-based Electronic, Optoelectronic and Electroacoustic Devices,” 2014, doi: 10.1038/srep03598.

[61] P. Avouris, “Graphene: Electronic and photonic properties and devices,” *Nano Lett.*, vol. 10, no. 11, pp. 4285–4294, Nov. 2010, doi: 10.1021/NL102824H/ASSET/IMAGES/LARGE/NL-2010-02824H_0006.JPEG.

[62] A. H. Castro Neto, F. Guinea, N. M. R. Peres, K. S. Novoselov, and A. K. Geim, “The electronic properties of graphene,” *Rev. Mod. Phys.*, vol. 81, no. 1, pp. 109–162, Jan. 2009, doi: 10.1103/REVMODPHYS.81.109/FIGURES/38/MEDIUM.

[63] K. F. Mak, M. Y. Sfeir, Y. Wu, C. H. Lui, J. A. Misewich, and T. F. Heinz, “Measurement of the opptical conductivity of graphene,” *Phys. Rev. Lett.*, vol. 101, no. 19, p. 196405, Nov. 2008, doi: 10.1103/PHYSREVLETT.101.196405/FIGURES/4/MEDIUM.

[64] L. Singh, M. Kumar, and S. Jain, “Electrically writable silicon nanophotonic resistive memory with inherent stochasticity,” *Opt. Lett. Vol. 44, Issue 16, pp. 4020-4023*, vol. 44, no. 16, pp. 4020–4023, Aug. 2019, doi: 10.1364/OL.44.004020.

[65] J. Mu, L. Chen, X. Li, W. P. Huang, L. C. Kimerling, and J. Michel, “Hybrid nano ridge plasmonic polaritons waveguides,” *Appl. Phys. Lett.*, vol. 103, no. 13, p. 131107, Sep. 2013, doi: 10.1063/1.4823546.

[66] “Light Assisted Electro-Metallization in Resistive Switch With Optical Accessibility.” https://opg.optica.org/jlt/abstract.cfm?uri=jlt-39-18-5869 (accessed May 12, 2022).

[67] L. Singh *et al.*, “Optical switch with ultra high extinction ratio using electrically controlled metal diffusion,” *Opt. Lett. Vol. 46, Issue 11, pp. 2626-2629*, vol. 46, no. 11, pp. 2626–2629, Jun. 2021, doi: 10.1364/OL.428710.

[68] A. Liu *et al.*, “A high-speed silicon optical modulator based on a metal–oxide–semiconductor capacitor,” *Nat. 2004 4276975*, vol. 427, no. 6975, pp. 615–618, Feb. 2004, doi: 10.1038/nature02310.

[69] A. K. Geim and K. S. Novoselov, “The rise of graphene,” *Nat. Mater.*

*2007 63*, vol. 6, no. 3, pp. 183–191, Mar. 2007, doi: 10.1038/nmat1849.

[70] M. Liu, X. Yin, and X. Zhang, "Double-layer graphene optical modulator," *Nano Lett.*, vol. 12, no. 3, pp. 1482–1485, Mar. 2012, doi: 10.1021/NL204202K/ASSET/IMAGES/LARGE/NL-2011-04202K_0005.JPEG.

[71] C. T. Phare, Y. H. Daniel Lee, J. Cardenas, and M. Lipson, "Graphene electro-optic modulator with 30 GHz bandwidth," *Nat. Photonics 2015 98*, vol. 9, no. 8, pp. 511–514, Jul. 2015, doi: 10.1038/nphoton.2015.122.

[72] C. Xu *et al.*, "Characteristics of electro-refractive modulating based on Graphene-Oxide-Silicon waveguide," *Opt. Express, Vol. 20, Issue 20, pp. 22398-22405*, vol. 20, no. 20, pp. 22398–22405, Sep. 2012, doi: 10.1364/OE.20.022398.

[73] M. Mohsin *et al.*, "Experimental verification of electro-refractive phase modulation in graphene," *Sci. Reports 2015 51*, vol. 5, no. 1, pp. 1–7, Jun. 2015, doi: 10.1038/srep10967.

[74] T. Mueller, F. Xia, and P. Avouris, "Graphene photodetectors for high-speed optical communications," *Nat. Photonics 2010 45*, vol. 4, no. 5, pp. 297–301, Mar. 2010, doi: 10.1038/nphoton.2010.40.

[75] D. Schall *et al.*, "50 GBit/s Photodetectors Based on Wafer-Scale Graphene for Integrated Silicon Photonic Communication Systems," *ACS Photonics*, vol. 1, no. 9, pp. 781–784, Sep. 2014, doi: 10.1021/PH5001605/SUPPL_FILE/PH5001605_SI_001.PDF.

[76] K. J. Vahala, "Optical microcavities," *Nat. 2003 4246950*, vol. 424, no. 6950, pp. 839–846, 2003, doi: 10.1038/nature01939.

[77] D. Liang *et al.*, "Electrically-pumped compact hybrid silicon microring lasers for optical interconnects," *Opt. Express, Vol. 17, Issue 22, pp. 20355-20364*, vol. 17, no. 22, pp. 20355–20364, Oct. 2009, doi: 10.1364/OE.17.020355.

[78] A. Agarwal *et al.*, "GHz-bandwidth optical filters based on high-order silicon ring resonators," *Opt. Express, Vol. 18, Issue 23, pp. 23784-23789*, vol. 18, no. 23, pp. 23784–23789, Nov. 2010, doi: 10.1364/OE.18.023784.

[79] Q. Xu, B. Schmidt, S. Pradhan, and M. Lipson, "Micrometre-scale silicon electro-optic modulator," *Nat. 2005 4357040*, vol. 435, no. 7040, pp. 325–327, May 2005, doi: 10.1038/nature03569.

[80] D. Chen, G. Wu, and M. Zhang, "Silicon hybrid plasmonic microring resonator for sensing applications," *Appl. Opt. Vol. 54, Issue 23, pp. 7131-7134*, vol. 54, no. 23, pp. 7131–7134, Aug. 2015, doi:

10.1364/AO.54.007131.

[81] C. Xiang, C.-K. Chan, and J. Wang, “Proposal and numerical study of ultra-compact active hybrid plasmonic resonator for sub-wavelength lasing applications,” 2014, doi: 10.1038/srep03720.

[82] Y. F. Xiao, B. B. Li, X. Jiang, X. Hu, Y. Li, and Q. Gong, “High quality factor, small mode volume, ring-type plasmonic microresonator on a silver chip,” *J. Phys. B At. Mol. Opt. Phys.*, vol. 43, no. 3, 2010, doi: 10.1088/0953-4075/43/3/035402.

[83] Y. Song, J. Wang, M. Yan, and M. Qiu, “Subwavelength hybrid plasmonic nanodisk with highQ factor and Purcell factor,” *J. Opt.*, vol. 13, no. 7, p. 075001, Apr. 2011, doi: 10.1088/2040-8978/13/7/075001.

[84] P. R. West, S. Ishii, G. V. Naik, N. K. Emani, V. M. Shalaev, and A. Boltasseva, “Searching for better plasmonic materials,” *Laser Photon. Rev.*, vol. 4, no. 6, pp. 795–808, Nov. 2010, doi: 10.1002/LPOR.200900055.

[85] D. I. Yakubovsky *et al.*, “Optical constants and structural properties of thin gold films,” *Opt. Express, Vol. 25, Issue 21, pp. 25574-25587*, vol. 25, no. 21, pp. 25574–25587, Oct. 2017, doi: 10.1364/OE.25.025574.

[86] P. Dastmalchi, A. Haddadpour, and G. Veronis, “Nanophotonics: devices for manipulating light at the nanoscale,” *Nanolithography Art Fabr. Nanoelectron. Nanophotonic Devices Syst.*, pp. 376–398, Jan. 2014, doi: 10.1533/9780857098757.376.

[87] M. Gould *et al.*, “Silicon-polymer hybrid slot waveguide ring-resonator modulator,” *Opt. Express, Vol. 19, Issue 5, pp. 3952-3961*, vol. 19, no. 5, pp. 3952–3961, Feb. 2011, doi: 10.1364/OE.19.003952.